

## A CO SURVEY OF REGIONS AROUND 34 OPEN CLUSTERS. II. PHYSICAL PROPERTIES OF CATALOGED MOLECULAR CLOUDS

D. LEISAWITZ<sup>1</sup>Laboratory for Astronomy and Solar Physics, NASA Goddard Space Flight Center; and  
Department of Astronomy, The University of Texas at Austin

Received 1989 October 10; accepted 1990 February 22

## ABSTRACT

Physical properties of the 148 molecular clouds found in a systematic survey of CO emission from regions around 34 young open clusters in the Milky Way are studied. Sources of bias and completeness of samples of clouds drawn from the catalog are discussed. The cloud size spectrum is found to be of the form  $N(R > R_0) \propto R_0^{-1.6}$  ( $8 \text{ pc} < R_0 < 20 \text{ pc}$ ), and the mass spectrum is given by  $N(M > M_0) \propto M_0^{-0.65}$  ( $2.0 \times 10^3 M_\odot < M_0 < 1.3 \times 10^5 M_\odot$ ). From nonlinear least-squares fits which take into account errors in observed parameters, two power-law scaling relations are measured:  $M \propto R^3$  and  $\Delta V \propto R^{0.6}$ , where  $\Delta V$  is the CO line width. The mass-radius relation implies that clouds of all sizes larger than a few pc have approximately the same mean volume density, about  $20 \text{ H}_2 \text{ cm}^{-3}$  assuming a standard CO intensity to  $\text{H}_2$  column density conversion factor. The clouds are not in virial equilibrium both in the sense that the observed CO lines are wider than  $V_{\text{vir}} = (3GM/5R)^{1/2}$ , and in that  $\Delta V/V_{\text{vir}}$  is a decreasing function of  $R$ . Molecular clouds associated with open clusters younger than 10 Myr are larger and more massive than, but have the same mean density as, the clouds associated with older clusters.

All the CO observations can be understood in terms of a model in which molecular clouds are thought of as ensembles of dense clumps. On the basis of such a model, it is demonstrated that molecular clouds are perturbed on a time scale short compared to the time required for them to reestablish virial equilibrium. The least certain parameter of the model characterizes the degree to which colliding clumps “remember” their trajectories; a prediction is made of its value based on the determination that clouds are not in equilibrium. The relatively small local dark clouds found in the survey of open cluster regions may resemble the clumps in larger clouds.

*Subject headings:* clusters: open — interstellar: molecules — stars: formation

## I. INTRODUCTION

It is not known whether molecular clouds in the Galaxy comprise a single population. If the stellar initial mass function is “bimodal” (see, e.g., Silk 1988, and references therein), different star formation mechanisms could be operative or distinct populations of progenitor clouds could exist. If there are distinct cloud populations, how can they be found? The issue becomes complicated when one attempts to sort out cause from effect. For example, the clouds from which massive stars form may appear to differ from other molecular clouds, but are they apparently unusual because of the influence of the stars, or were they substantially different to begin with?

Of great interest also are questions regarding the dynamic stability of interstellar clouds. What is the lifetime of a molecular cloud? Do the clouds exist in a steady state until they are destroyed by the stars they produce? Lacking a theory of compressible turbulence in a dynamically evolving system (see Fleck 1983), one must depend upon hydrodynamic and  $N$ -body simulations (e.g., see Gilden 1984; Hausman 1981; Pumphrey and Scalo 1983; Stone 1970), to guide one’s intuition and one must recognize the limitations of those simulations, sophisticated as they may be. Cloud structure has been studied as well (e.g., David and Verschueren 1987; Kleiner and Dickman 1985; Scalo 1987, and references therein; Terebey *et al.* 1986). Observational studies of large cloud samples (e.g., Casoli, Combes, and Gerin 1984; Clemens and Barvainis 1988; Dame *et al.* 1986, 1987; Sanders, Scoville, and Solomon 1985;

Solomon *et al.* 1987), and parallel investigations of the structure and dynamic stability of individual clouds (e.g., Frerking, Langer, and Wilson 1987), have catalyzed the development of the theory.

Many of the observations suggest that molecular clouds are supported against self-gravitational collapse by turbulent pressure (see, e.g., Larson 1981), possibly assisted by magnetic fields (see, e.g., Myers and Goodman 1988). A number of investigations have focused on how a state of virial equilibrium might be maintained (e.g., Bash, Hausman, and Papaloizou 1981; Chièze 1987; Elmegreen 1989; Fleck 1988; Kleiner and Dickman 1985; Leung, Kutner, and Mead 1982; Norman and Silk 1980; Scalo and Pumphrey 1982), or on why clouds might appear to be in virial equilibrium even if they are not (e.g., Kegel 1989; Maloney 1988).

Although we are not prepared to answer decisively the questions raised above, we will address some relevant issues by examining the physical characteristics of a large number of molecular clouds, some of which were recent sites of massive star formation. The clouds were cataloged by Leisawitz, Bash, and Thaddeus (1989, hereafter Paper I), who surveyed regions around 34 young open clusters for carbon monoxide (CO) spectral line emission. A total of 148 resolved molecular clouds were found in the  $110 \text{ deg}^2$  survey area. Some of our empirical results, especially the relationship of cloud mass to cloud size, differ from those reported elsewhere. Our interpretation of the observations also differs from most others in that we consider the possibility that molecular clouds are kept out of virial equilibrium by the injection of mechanical energy on a time

<sup>1</sup> USRA Resident Research Associate.

scale short compared to the relevant dynamical relaxation time.

For several reasons, the open cluster CO survey is well suited for the proposed analysis. First, most of the surveyed regions are in the outer Galaxy, where chance superposition of clouds along a line of sight is uncommon; individual clouds are readily distinguishable. Second, the survey is systematic: the same instrumentation is used throughout, the integration time is adjusted to maintain constant sensitivity, and the spatial sampling is uniform. Third, the distances and, perhaps, ages of the clouds are known. The distances of clouds associated with open clusters are known with high relative accuracy compared to the distances of most other interstellar clouds because the cluster distances, which are based on main-sequence fitting of photometric data, can be used. Since the cluster luminosities and ages (time elapsed since the formation of massive stars) are known from the cluster main-sequence turnoff, the radiative and dynamical influence a cluster has on a nearby molecular cloud can be ascertained. Fourth, it is possible to exploit the fact that not all the clouds observed in the cluster survey are associated with a cluster to compare clouds that recently formed massive stars with others that have not done so.

The reader will find in § II a description of the open cluster CO survey and the method used to isolate molecular clouds and measure their properties. In § III, the cloud properties are tabulated and summarized, and the issue of catalog completeness is addressed. Empirical relations of CO line width and cloud mass to cloud size are derived and interpreted in § IV. Characteristics of the clouds believed to be associated with young open clusters are discussed in § V. Section VI contains a summary of our findings which are, briefly, that CO line width and cloud mass obey power-law scaling relations with cloud size, that clouds of all sizes have approximately the same volume density, that molecular clouds are not in virial equilibrium, and that clouds associated with extremely young star clusters are larger and more massive than clouds associated with older clusters. Later papers will focus on analysis of the shapes of molecular clouds found in the open cluster CO survey (David and Leisawitz 1990) and tabulation and discussion of the infrared properties of the clouds.

## II. OBSERVATIONS AND DATA REDUCTION

The open cluster CO survey, which was carried out with the Columbia-GISS 1.2 m millimeter-wave telescope, is described at length in Paper I. Therefore, we review here only those aspects of the observing technique and data processing procedure that relate directly to the discovery and characterization of the molecular clouds.

Tables 1 and 2 summarize the survey. All CO observations discussed in this paper are of emission in the 2.6 mm  $J = 1 \rightarrow 0$  line of the normal isotopic species,  $^{12}\text{C}^{16}\text{O}$ . Table 1 lists the survey resolution, sampling, sensitivity, etc. The coverage of the survey is given in Table 2 (also see Fig. 1 of Paper I). The data were calibrated using the method described by Kutner and Ulich (1981), with the two-layer atmosphere model of Kutner (1978). In the conventional notation, the CO line radiation temperature,  $T_R^* = T_A^*/\eta_{\text{FSS}}$ , where  $T_A^*$  represents the antenna temperature, and the efficiency factor  $\eta_{\text{FSS}}$ , shown in Table 1, adjusts for spillover and scattering of the feed-horn power beyond the main beam of the telescope.

To reduce the data, we adopt the following practical definition: a "molecular cloud" is an object that produces a CO spectral emission feature detectable in at least two contiguous

TABLE 1

SURVEY DESCRIPTION AND TELESCOPE PARAMETERS AT 115 GHz

Parameter	Value
Spectral line	$^{12}\text{C}^{16}\text{O} (J = 1 \rightarrow 0)$
Rest frequency	115.271291 GHz
Telescope	Columbia-GISS 1.2 m (New York City)
Antenna resolution <sup>a</sup>	8.7
Pointing uncertainty	<1'
Sampling interval	7.5
Map coordinates	Galactic
Total survey coverage	$\sim 110 \text{ deg}^2$
Velocity resolution	$0.65 \text{ km s}^{-1}$
Spectrometer range <sup>b</sup>	$166 \text{ km s}^{-1}$
Receiver noise temperature <sup>c</sup>	85 K
Integration time per scan	$\sim 45 \text{ s}$
RMS baseline noise	0.28 K ( $T_A^*$ )
Beam efficiency, $\eta_{\text{FSS}}$	0.82
Line intensity repeatability	6% <sup>d</sup>

<sup>a</sup> Full beamwidth at half-power (HPBW).

<sup>b</sup> Centered on radial velocity of target cluster.

<sup>c</sup> Single sideband.

<sup>d</sup> rms deviation based on daily observations of a standard source (Dame 1988, private communication).

observed positions at a common radial velocity. In principle, the definition could be relaxed to include spatially unresolved clouds, but the physical properties of such clouds cannot be measured because of the uncertain way in which they couple to

TABLE 2

SURVEY COVERAGE

CLUSTER AT MAP CENTER		CLUSTER COORDINATES		
OCL Number <sup>a</sup>	Common Name	$l$	$b$	MAP DIAMETER
67	NGC 6694	23:86	-2:92	2:625
100	NGC 6709	42.16	+4.70	3.125
124	NGC 6823	59.41	-0.15	2.125
138	Roslund 4	66.96	-1.26	1.625
205	NGC 7062	89.93	-2.72	1.625
208	NGC 7067	91.19	-1.67	1.125
222	IC 1396	99.29	+3.73	3.625
224	IC 1442	101.36	-2.20	1.625
236	NGC 7160	104.02	+6.45	3.125
244	NGC 7380	107.08	-0.90	2.125
286	Bk 59	118.25	+4.95	3.125
291	NGC 103	119.80	-1.38	1.125
313	NGC 281	123.13	-6.24	1.625
314	Bk 62	123.99	+1.10	1.625
319	NGC 433	125.90	-2.60	1.125
320	NGC 436	126.07	-3.91	1.625
321	NGC 457	126.56	-4.35	2.125
333	NGC 663	129.46	-0.94	2.625
339	Stock 5	130.74	+2.65	2.625
345	NGC 744	132.39	-6.16	2.125
362	NGC 957	136.34	-2.66	2.125
364	IC 1848	137.19	+0.92	2.125
394	NGC 1444	148.16	-1.29	3.125
403	NGC 1624	155.35	+2.58	1.125
404	Bk 11	157.08	-3.65	1.625
406	NGC 1605	158.61	-1.58	1.125
429	NGC 1778	168.88	-2.00	2.125
439	NGC 1893	173.59	-1.70	2.125
441	NGC 1931	173.90	+0.28	1.625
467	NGC 2129	186.61	+0.13	1.625
476	NGC 2175	190.20	+0.42	3.125
	Monoceros	218.00	-0.50	1.125

<sup>a</sup> Open cluster number from the catalog of Alter, Ruprecht, and Vanysek 1970.

the telescope beam. To search for the clouds in a region covered by the open cluster CO survey, a series of at least 15 contour maps, each showing the CO line emission integrated over three filterbank channels ( $\sim 2 \text{ km s}^{-1}$ ), is produced (see Fig. 12 of Paper I). The series of maps spans a range of radial velocity at least  $\pm 15 \text{ km s}^{-1}$  centered on the velocity of the targeted star cluster; data at other velocities are examined in the same manner when additional emission is found on inspection of the raw spectral data.

When the presence of a cloud is signaled by the discovery of spatially extended CO emission at the  $1 \text{ K km s}^{-1}$  ( $3.2 \sigma$ ) level in the three-channel maps, a new contour map is generated to show the emission integrated over the cloud's full extent in velocity. The ratio of velocity-integrated CO line intensity to baseline noise is maximized in this way, since the integration excludes emission-free portions of baseline. The cloud is represented as an ellipse, and its major and minor axes are measured as described in Paper I; the center of the cloud, for the purpose of describing its location, is considered to be the point of intersection of these axes. Whenever a cloud radius is discussed in this paper, it is half the geometric mean of the major and minor axis lengths.

The CO spectral line flux of a molecular cloud,  $S_{\text{CO}}$ , is given by

$$S_{\text{CO}} = \sum \left( \int T_{\text{R}}^* dv \right)_i, \quad (1)$$

where the summation ranges from  $i = 1$  to  $N$ , the total number of lines of sight containing emission from the cloud. The CO line luminosity,  $L_{\text{CO}}$ , is derived from

$$L_{\text{CO}} = 8\pi A k \left\langle \int T_{\text{R}}^* dv \right\rangle / \lambda^3 \\ \simeq 1.5 \times 10^{-2} d^2 S_{\text{CO}} L_{\odot}, \quad (2)$$

where  $A$  is the projected area of the cloud and  $\lambda$  is the rest wavelength of the CO line. The numerical coefficient in equation (2) is applicable when the cloud distance,  $d$ , is given in kiloparsecs and  $S_{\text{CO}}$  is expressed in units of  $\text{K km s}^{-1} \text{ deg}^2$ . With the assumption that the molecular hydrogen column density is related to the CO line intensity by

$$N(\text{H}_2) \simeq 1.9 \times 10^{20} \text{ cm}^{-2} \text{ K}^{-1} \text{ km}^{-1} \text{ s} \int T_{\text{R}}^* dv \quad (3)$$

(see, e.g., Strong *et al.* 1988), the molecular cloud mass is given by

$$M = \mu X \lambda^3 L_{\text{CO}} / 8\pi k, \quad (4a)$$

or

$$\left( \frac{M}{M_{\odot}} \right) \simeq 8.4 \times 10^4 \left( \frac{L_{\text{CO}}}{L_{\odot}} \right), \quad (4b)$$

where  $X$  is the coefficient in equation (3). This coefficient differs from the value derived by Strong *et al.* in compensation for the slightly different value of  $\eta_{\text{FSS}}$  that we adopt for the Columbia-GISS telescope. The velocity-integrated *antenna* temperature ( $T_{\text{A}}^*$ ), the quantity actually measured at the telescope, is assumed to be related to  $N(\text{H}_2)$  by the *same* constant of proportionality as that derived by Strong *et al.* The helium contribution to the mass of the cloud is taken into account in equation (4) using a mean molecular weight per  $\text{H}_2$  molecule,

$\mu$ , of 2.72 amu, equivalent to a helium-to-hydrogen ratio, by number, of 0.09 (Allen 1973).

An integrated, or composite, CO spectrum is derived for each cloud:

$$T_j = \sum [T_{\text{R}}^*(v_j)]_i, \quad i = 1, N. \quad (5)$$

From this spectrum, the mean radial velocity of the cloud is obtained using the relation

$$\langle V \rangle = \sum (v_j T_j) / \sum T_j. \quad (6)$$

The composite CO line equivalent width is obtained from

$$\Delta V_{\text{eqw}} = \frac{\Delta v_{\text{ch}} \sum T_j}{T_j(\text{max})}. \quad (7)$$

In equations (6) and (7), the summation is over the spectrometer channels containing emission from the cloud. The channel width,  $\Delta v_{\text{ch}}$ , is  $0.65 \text{ km s}^{-1}$  (see Table 1), and  $T_j(\text{max})$  is the peak temperature in the composite line profile. The full CO line width at half maximum would be  $\Delta V_{\text{FWHM}} = 0.94 \Delta V_{\text{eqw}}$  if the line were Gaussian.

### III. THE CLOUD CATALOG

In this section, properties of the molecular clouds found in the survey are tabulated, and selection effects that limit the ranges of observed cloud properties are discussed.

#### a) Compilation of Measured and Derived Cloud Properties

Physical characteristics of the 148 molecular clouds found in the CO survey data are given in Tables 3 and 4. The cloud names, from Paper I, derive from the names of the clusters near which they are found. Table 3 contains positional information: Galactic coordinates of the cloud center, radial velocity relative to the local standard of rest (LSR), angular extents of the major and minor axes, and Galactic position angle (GPA) of the major axis measured counterclockwise with GPA = 0 corresponding to a vector parallel to the Galactic plane that points toward decreasing Galactic longitude. Also given in Table 3 is an indication of whether the map of a cloud is complete (C) or, apparently, incomplete (I). A cloud is considered to be completely mapped if the lowest significant CO intensity contour (usually  $1 \text{ K km s}^{-1}$ ) is closed within the survey boundary. Forty-three of the cataloged clouds (29%) had been detected previously in the Columbia-GISS large-scale CO survey of the Galactic plane (Dame *et al.* 1987).

The clouds are classified as follows: "A" for clouds that can be confidently associated with the clusters near which they are located; "L" for local dark clouds; "U" for clouds considered to be associated with young stellar objects other than the targeted clusters; and "a" for the remaining clouds, which may or may not be associated with the nearby clusters. Since the clusters surveyed are more distant than  $\sim 1 \text{ kpc}$ , the local dark clouds, which have LSR velocities near zero and correspond to regions of exceptionally low star density on the Palomar Observatory Sky Survey (POSS) prints, indubitably are not associated with the clusters. Only clouds that show clear evidence of interaction with a cluster, usually a "bright rim" due to exposure to a cluster's ionizing radiation, are assigned to category A (see Paper I). The cloud classifications are listed in Tables 3 and 4. Of the 148 clouds cataloged, 20 (14%) are in class A, 42 (28%) are in class L, 9 (6%) are in class U, and 77 (52%) are in class a.

Distances are adopted for the clouds consistent with their

TABLE 3  
CLASSIFICATIONS, LOCATIONS, AND ORIENTATIONS OF MOLECULAR CLOUDS

CLOUD	I/C	CLASS	CENTER POSITION		$\langle V \rangle$ (km s <sup>-1</sup> )	$\sigma_{\langle V \rangle}$ (km s <sup>-1</sup> )	$a_{\min}$	$a_{\max}$	GPA
			<i>l</i>	<i>b</i>					
NGC 6694A .....	C	L	024°4	-02°5	9.5	0.8	0°53	0°84	-12°
NGC 6694B .....	C	L	024.1	-03.3	8.7	0.7	0.46	1.30	-4
NGC 6694C .....	I	L	023.8	-02.0	8.3	1.1	0.97	1.24	2
NGC 6694D .....	C	L	023.2	-02.4	8.2	0.5	0.41	0.55	78
NGC 6694E .....	C	L	022.9	-02.9	7.8	0.7	0.89	0.96	-4
NGC 6694F .....	C	L	023.4	-03.7	10.1	0.4	0.19	0.65	-15
NGC 6694G .....	I	L	023.7	-04.2	8.8	1.2	0.35	0.35	...
NGC 6709A .....	I	U	041.4	+03.8	27.5	1.2	0.79	2.01	45
NGC 6709B .....	C	U	042.9	+03.8	31.1	1.7	0.29	1.04	-30
NGC 6709C .....	I	a	042.1	+03.3	5.7	0.13	0.20	0.45	38
NGC 6823A .....	C	A	059.3	-00.3	25.3	1.2	0.62	1.83	-35
NGC 6823B .....	C	a	059.1	-00.3	32.0	1.2	0.63	1.48	-5
NGC 6823C .....	I	a	058.5	+00.5	34.8	2.1	0.61	0.83	-48
NGC 6823D .....	I	a	060.2	-00.5	28.8	0.54	0.53	0.82	30
NGC 6823E .....	C	a	059.8	-00.8	23.7	2.4	0.53	0.66	56
Roslund 4A .....	C	L	066.9	-01.3	4.3	0.6	0.70	1.03	0
Roslund 4B .....	I	a	066.6	-01.1	13.0	1.9	0.78	1.92	-87
NGC 7062A .....	I	L	090.7	-02.4	3.6	0.94	0.43	0.54	51
NGC 7062B .....	I	L	089.9	-02.2	3.8	1.3	0.56	1.36	32
NGC 7062C .....	I	L	089.3	-02.7	1.4	0.4	0.35	0.79	-31
NGC 7067A .....	C	L	091.1	-01.5	0.2	0.3	0.31	0.63	53
NGC 7067B .....	I	L	090.7	-01.5	4.9	0.6	0.48	0.89	-65
NGC 7067C .....	C	L	091.3	-01.9	4.5	0.28	0.20	0.20	...
NGC 7067D .....	I	L	091.2	-02.1	4.3	0.46	0.37	0.67	25
NGC 7067E .....	I	a	090.8	-01.4	-20.0	0.80	0.19	0.33	-67
IC 1396A .....	C	A	098.9	+04.2	-6.8	2.0	0.52	0.90	48
IC 1396B .....	C	A	100.3	+03.2	-2.2	1.0	0.87	1.58	-37
IC 1396C .....	I	a	098.3	+05.0	-0.7	0.91	0.61	1.01	-82
IC 1396D .....	I	a	099.3	+05.3	-1.0	0.57	0.68	1.26	21
IC 1396E .....	C	A	100.0	+04.5	-0.3	0.68	0.87	1.78	-50
IC 1396F .....	C	L	098.1	+03.2	7.6	0.97	1.31	1.60	59
IC 1442A .....	C	U	101.4	-02.6	-29.8	0.37	0.25	0.25	...
NGC 7160A .....	C	a	104.9	+07.3	-11.4	1.6	0.33	0.87	4
NGC 7160B .....	C	a	104.2	+07.3	-12.5	3.5	0.45	1.03	-44
NGC 7160C .....	C	a	104.4	+06.4	-0.9	2.3	0.21	1.14	-37
NGC 7160D .....	C	a	103.8	+05.7	-0.0	0.63	0.33	0.48	66
NGC 7160E .....	C	a	103.2	+05.8	-5.3	0.35	0.21	0.48	-35
NGC 7160F .....	I	a	103.9	+05.1	-0.9	0.55	0.49	0.62	-89
NGC 7160G .....	C	a	103.4	+06.4	-5.9	0.67	0.25	0.60	-45
NGC 7160H .....	C	a	103.2	+07.0	-2.4	0.92	0.65	0.88	-77
NGC 7160I .....	C	a	102.9	+07.3	-6.8	0.22	0.23	0.23	...
NGC 7160J .....	I	a	102.8	+05.4	-2.9	0.52	0.26	0.58	49
NGC 7160K .....	C	a	104.4	+07.8	-9.7	2.1	0.12	0.21	84
NGC 7160L .....	C	a	105.4	+06.1	-4.3	3.3	0.17	0.52	-44
NGC 7160M .....	C	a	104.0	+07.6	-24.6	2.8	0.19	0.93	-15
NGC 7160N .....	C	a	104.9	+06.8	-24.3	2.6	0.30	0.54	54
NGC 7160O .....	C	a	104.6	+05.8	-20.2	1.7	0.19	0.30	-76
NGC 7160P .....	C	a	103.3	+06.7	-20.6	1.7	0.16	0.48	1
NGC 7160Q .....	C	a	103.3	+05.7	-19.9	3.0	0.45	0.63	-31
NGC 7160R .....	C	a	104.3	+06.6	-23.6	1.5	0.30	0.37	23
NGC 7380A .....	I	a	106.6	-00.1	-55.3	0.95	0.54	0.84	-47
NGC 7380B .....	I	a	107.8	-01.4	-53.5	0.94	0.33	1.01	-46
NGC 7380C .....	C	a	106.3	-00.9	-54.3	0.67	0.32	0.49	22
NGC 7380D .....	I	a	107.5	-00.1	-50.2	1.1	0.57	1.08	21
NGC 7380E .....	C	A	107.1	-01.0	-41.4	1.6	0.30	1.20	-27
NGC 7380F .....	I	L	107.2	-00.1	-3.5	0.50	0.53	0.73	90
Bk 59A .....	C	A	117.5	+05.2	-13.6	1.9	0.79	1.81	12
Bk 59B .....	I	a	118.2	+03.3	-17.8	0.61	0.46	0.57	0
Bk 59C .....	I	A	118.0	+04.0	-6.6	1.1	1.05	3.10	24
Bk 59D .....	C	A	118.0	+04.8	-0.8	1.2	0.74	1.20	-18
Bk 59E .....	I	A	119.2	+05.4	-8.1	1.2	1.63	2.48	53
NGC 103A .....	I	a	119.4	-01.6	-34.9	2.1	0.26	0.70	87
NGC 281A .....	C	A	123.4	-06.4	-30.4	1.1	0.74	1.11	6
NGC 281B .....	C	a	122.7	-06.3	-44.0	0.64	0.44	0.86	-64
Bk 62A .....	I	a	124.3	+00.5	-45.1	0.76	0.46	0.46	...
Bk 62B .....	I	L	124.2	+01.8	-8.7	1.1	0.75	0.84	-22
Bk 62C .....	C	a	124.0	+00.7	-12.5	0.87	0.41	0.76	61
NGC 433A .....	I	a	125.4	-02.6	-22.7	0.76	0.43	0.59	28
NGC 433B .....	I	a	126.0	-02.1	-21.6	0.29	0.32	0.61	-43
NGC 433C .....	C	a	126.3	-02.6	-10.9	0.42	0.32	0.80	0
NGC 433D .....	I	a	125.8	-02.2	-10.7	0.34	0.31	0.83	-78
NGC 663A .....	I	a	129.1	-00.0	-34.9	1.9	0.98	1.48	34
NGC 663B .....	I	a	130.7	-00.9	-32.9	0.85	0.60	0.88	22
NGC 663C .....	I	a	128.9	-00.3	-13.6	1.6	1.41	2.26	-38

TABLE 3—Continued

CLOUD	I/C	CLASS	CENTER POSITION		$\langle V \rangle$ (km s <sup>-1</sup> )	$\sigma_{\langle V \rangle}$ (km s <sup>-1</sup> )	$a_{\min}$	$a_{\max}$	GPA
			$l$	$b$					
NGC 663D	C	L	129.3	-01.6	-10.9	0.87	0.44	1.19	-43
NGC 663E	I	L	129.7	-02.2	-13.2	0.40	0.31	0.71	-26
NGC 663F	I	L	130.5	-00.9	-10.5	1.9	0.43	0.85	28
NGC 663G	I	L	128.2	-00.8	3.3	1.3	0.69	1.41	74
NGC 663H	C	L	129.6	-00.2	3.5	1.8	0.50	0.99	74
Stock 5A	C	a	130.6	+03.3	-6.6	0.54	0.33	0.84	-18
Stock 5B	C	a	130.7	+02.9	-8.1	0.13	0.19	0.56	87
Stock 5C	I	a	131.7	+02.8	-7.4	0.49	0.71	1.12	-42
Stock 5D	I	a	130.1	+03.8	-1.7	0.79	0.79	1.73	-17
Stock 5E	C	a	130.2	+02.8	-4.8	0.62	0.34	0.39	74
Stock 5F	C	a	130.3	+02.2	-4.4	0.55	0.23	0.31	-45
Stock 5G	C	a	129.8	+02.1	-3.1	0.44	0.29	0.47	-66
Stock 5H	C	a	131.4	+02.2	0.8	0.36	0.50	1.52	-37
Stock 5I	I	a	129.9	+02.2	1.1	0.52	1.05	1.54	-4
NGC 744A	C	a	132.0	-06.1	-18.0	1.1	0.21	0.23	-57
NGC 744B	C	a	132.1	-05.7	-10.4	1.9	0.53	0.19	-53
NGC 744C	C	a	132.6	-06.0	-10.4	2.3	0.32	0.99	-34
NGC 744D	C	a	131.6	-06.0	-4.3	0.64	0.43	0.54	79
NGC 957A	I	L	136.3	-02.0	-10.8	1.22	1.16	1.55	-56
IC 1848A	C	A	136.7	+01.3	-38.2	1.7	0.85	1.56	-42
IC 1848B	C	A	137.7	+01.4	-39.0	1.6	0.44	0.78	-61
IC 1848C	C	A	138.1	+00.8	-38.1	0.39	0.29	0.43	17
IC 1848D	I	L	136.2	+00.5	-12.6	1.4	0.26	0.66	-46
IC 1848E	C	A	137.4	+00.7	-38.2	3.0	0.30	0.47	45
IC 1848F	C	L	137.1	+00.5	-10.9	0.77	0.30	0.30	...
IC 1848G	I	a	136.9	+00.2	-34.7	4.3	0.15	0.60	72
NGC 1444A	C	U	148.8	-01.3	-26.0	0.36	0.35	0.39	9
NGC 1444B	C	a	148.2	-01.5	-25.4	0.43	0.44	0.56	-79
NGC 1444C	C	L	147.0	-01.5	-10.9	0.62	0.24	0.26	-84
NGC 1444D	C	L	149.2	-02.1	-8.8	0.54	0.57	0.77	-65
NGC 1444E	I	L	149.6	-01.1	-8.1	1.00	0.53	1.25	78
NGC 1444F	C	L	147.9	-01.8	-6.2	0.94	0.32	0.50	70
NGC 1444G	C	U	147.5	-00.4	-7.2	1.2	0.43	0.79	3
NGC 1444H	I	U	148.3	-00.3	-3.7	1.5	0.88	1.76	1
NGC 1444I	C	L	149.2	-00.4	-4.5	0.24	0.33	0.47	-67
NGC 1444J	C	L	147.6	-01.2	-0.4	0.56	0.74	1.43	30
NGC 1444K	I	a	147.3	-02.5	0.2	0.35	0.40	0.82	29
NGC 1444L	C	a	146.9	-01.4	5.5	0.75	0.25	0.51	28
NGC 1624A	I	U	154.9	+02.6	-37.0	1.1	0.44	0.59	90
NGC 1624B	C	A	155.5	+02.6	-36.7	0.82	0.36	0.77	-68
NGC 1624C	I	L	155.6	+03.0	0.6	0.63	0.32	0.54	4
NGC 1624D	I	L	154.9	+02.6	0.0	0.48	0.45	1.16	75
Bk 11A	I	a	156.9	-03.0	-30.7	1.2	0.51	0.91	-49
Bk 11B	C	a	157.3	-04.0	-31.6	0.97	0.62	1.21	41
Bk 11C	C	a	156.8	-03.1	-22.1	0.33	0.14	0.38	-41
Bk 11D	I	L	157.1	-02.9	-8.1	0.49	0.62	1.11	81
Bk 11E	I	L	157.2	-03.0	-0.9	0.37	0.23	0.69	-65
Bk 11F	I	a	157.8	-04.0	-1.1	0.54	0.26	0.35	-71
Bk 11G	I	a	157.3	-04.3	-9.1	0.21	0.21	0.25	67
NGC 1605A	I	a	158.6	-01.9	-26.0	1.1	0.56	1.04	-6
NGC 1605B	I	L	158.5	-01.1	-3.4	1.1	0.38	0.49	70
NGC 1778A	I	L	168.4	-01.1	-15.3	1.2	0.52	0.90	-41
NGC 1778B	I	L	169.7	-01.5	-8.5	0.73	0.72	0.93	63
NGC 1778C	I	L	168.8	-01.2	-10.7	0.84	0.68	1.56	-44
NGC 1778D	I	L	169.3	-02.8	5.7	0.26	0.25	0.38	45
NGC 1893A	C	A	174.0	-01.9	-6.0	1.3	0.57	1.50	24
NGC 1893B	C	a	173.4	-02.6	-5.7	1.8	0.15	0.25	35
NGC 1893C	C	a	173.2	-01.3	-3.6	2.5	0.21	0.45	-57
NGC 1893D	I	a	172.6	-01.4	-8.2	0.86	0.36	0.50	-67
NGC 1893E	C	a	173.9	-01.0	-7.2	0.74	0.25	0.54	26
NGC 1931A	I	a	174.3	+00.9	-18.4	0.47	0.26	0.66	90
NGC 1931B	C	U	173.5	+00.0	-13.9	0.76	0.34	0.61	-62
NGC 1931C	I	A	174.3	-00.1	-3.3	0.99	0.41	1.18	47
NGC 2129A	I	a	187.1	-00.2	1.3	1.2	0.78	0.93	-42
NGC 2129B	C	a	186.7	+00.2	4.3	0.76	0.36	0.67	37
NGC 2129C	I	a	186.0	-00.1	6.3	0.41	0.61	1.32	77
NGC 2175A	I	U	189.1	+01.1	4.2	1.3	1.15	1.30	60
NGC 2175B	C	A	190.0	-00.1	7.4	1.2	1.02	1.60	63
NGC 2175C	C	a	189.7	-00.7	6.7	2.8	0.31	0.72	67
NGC 2175D	I	a	191.6	+01.3	-0.6	0.69	0.37	0.60	58
NGC 2175E	I	a	190.3	+01.4	0.3	0.37	0.37	0.94	-81
NGC 2175F	C	L	190.9	-00.6	-0.5	0.70	0.31	1.30	0
NGC 2175G	C	A	191.1	+00.4	7.2	1.8	1.07	2.01	49
Monoceros A	C	A	218.0	-00.3	27.3	1.5	0.45	1.00	34

TABLE 4  
PHYSICAL PROPERTIES OF MOLECULAR CLOUDS

Cloud	Class	$S_{\text{CO}}$ (K km s <sup>-1</sup> )	$\sigma_{S_{\text{CO}}}$ (K km s <sup>-1</sup> )	$N$	$V_{\text{eqw}}$ (km s <sup>-1</sup> )	$\sigma_V$ (km s <sup>-1</sup> )	$d$ (kpc)	$a_{\text{min}}$ (pc)	$a_{\text{maj}}$ (pc)	$\frac{c_{\text{min}}}{a_{\text{maj}}}$	$L_{\text{CO}}$ ( $L_{\odot}$ )	$M$ ( $10^3 M_{\odot}$ )	Peak $T_R^*$ (K)	Peak $N(\text{H}_2)$ ( $10^{20} \text{ cm}^{-2}$ )
NGC 6694A	L	2.9	0.07	29	4.55	0.03	0.20	1.9	2.9	0.63	0.0017	0.14	3.5	21.
NGC 6694B	L	3.2	0.08	41	3.37	0.03	0.20	1.6	4.5	0.35	0.0019	0.16	2.8	20.
NGC 6694C	L	6.2	0.10	55	4.34	0.02	0.20	3.4	4.3	0.78	0.0037	0.31	4.0	27.
NGC 6694D	L	1.2	0.05	14	5.23	0.04	0.20	1.4	1.9	0.75	0.00072	0.060	2.8	19.
NGC 6694E	L	1.9	0.07	33	4.35	0.04	0.20	3.1	3.4	0.93	0.0011	0.096	2.0	12.
NGC 6694F	L	0.72	0.05	17	2.65	0.07	0.20	0.7	2.3	0.29	0.00043	0.036	2.6	10.
NGC 6694G	L	0.27	0.04	8	4.80	0.15	0.20	1.2	1.2	1.00	0.00016	0.014	2.6	6.3
NGC 6709A	U	2.3	0.14	61	5.10	0.06	2.20	30	77	0.39	0.16	14.	1.7	11.
NGC 6709B	U	1.2	0.10	29	5.78	0.09	2.20	11	40	0.28	0.090	7.5	1.8	11.
NGC 6709C	a	0.21	0.03	7	1.94	0.15	0.93	3.2	7.3	0.44	0.0027	0.23	2.0	7.0
NGC 6823A	A	11.1	0.11	89	8.11	0.01	2.70	29	86	0.34	1.2	100.	9.3	79.
NGC 6823B	a	11.7	0.11	55	4.53	0.01	2.70	30	70	0.43	1.3	110.	8.3	75.
NGC 6823C	a	7.6	0.08	17	16.92	0.01	2.70	29	39	0.73	0.83	69.	4.5	101.
NGC 6823D	a	1.2	0.04	22	4.97	0.04	2.70	25	39	0.65	0.13	11.	3.2	18.
NGC 6823E	a	1.3	0.06	19	6.92	0.05	2.70	25	31	0.80	0.14	12.	2.2	20.
Roslund 4A	L	3.4	0.07	48	3.03	0.02	0.40	4.9	7.2	0.68	0.00082	0.69	3.5	21.
Roslund 4B	a	9.0	0.13	73	8.65	0.02	2.90	39	97	0.41	1.1	95.	4.8	38.
NGC 7062A	L	0.37	0.03	6	3.73	0.09	0.83	6.2	7.8	0.80	0.0038	0.32	3.3	13.
NGC 7062B	L	5.6	0.08	39	4.85	0.02	0.83	8.1	20	0.41	0.058	4.9	6.3	36.
NGC 7062C	L	0.97	0.05	14	2.23	0.05	0.83	5.1	11	0.44	0.010	0.84	4.8	17.
NGC 7067A	L	0.46	0.02	13	1.86	0.05	0.83	4.5	9.1	0.49	0.0047	0.40	3.4	9.3
NGC 7067B	L	0.97	0.04	17	2.97	0.05	0.83	7.0	13	0.54	0.010	0.84	2.7	23.
NGC 7067C	L	0.12	0.02	6	1.55	0.18	0.83	2.9	2.9	1.00	0.0012	0.10	2.3	7.0
NGC 7067D	L	0.34	0.03	11	2.98	0.09	0.83	5.4	9.7	0.55	0.0035	0.29	2.3	6.5
NGC 7067E	a	0.16	0.03	4	3.06	0.20	3.50	12	20	0.58	0.029	2.5	1.7	8.8
IC 1396A	A	1.8	0.07	26	4.04	0.04	0.80	7.3	13	0.58	0.017	1.4	4.1	25.
IC 1396B	A	5.6	0.09	57	3.49	0.02	0.80	12	22	0.55	0.053	4.5	6.2	38.
IC 1396C	a	2.9	0.06	29	4.17	0.02	0.80	8.5	14	0.60	0.028	2.3	3.9	23.
IC 1396D	a	2.2	0.06	38	3.08	0.03	0.80	9.5	18	0.54	0.021	1.8	3.5	14.
IC 1396E	A	6.9	0.09	83	2.84	0.02	0.80	12	25	0.49	0.066	5.5	3.5	25.
IC 1396F	L	9.2	0.16	120	3.37	0.02	0.40	9.1	11	0.82	0.022	1.9	5.2	29.
IC 1442A	U	0.40	0.05	9	2.74	0.13	3.00	13	13	1.00	0.054	4.5	2.0	9.5
NGC 7160A	a	1.0	0.06	17	4.64	0.06	0.70	4.0	11	0.38	0.0073	0.61	2.9	16.
NGC 7160B	a	1.1	0.08	25	5.15	0.07	0.70	5.5	13	0.44	0.0080	0.68	2.9	13.
NGC 7160C	a	1.0	0.08	30	2.30	0.08	0.70	2.6	14	0.18	0.0073	0.61	2.7	9.3
NGC 7160D	a	0.43	0.05	12	2.45	0.12	0.70	4.0	5.9	0.69	0.0031	0.26	2.1	8.6
NGC 7160E	a	0.21	0.04	7	2.59	0.20	0.70	2.6	5.9	0.44	0.0015	0.13	1.2	5.6
NGC 7160F	a	0.53	0.05	13	2.25	0.10	0.70	6.0	7.6	0.79	0.0039	0.33	2.4	12.
NGC 7160G	a	0.53	0.06	15	4.69	0.12	0.70	3.1	7.3	0.42	0.0039	0.33	1.3	8.6
NGC 7160H	a	0.99	0.08	27	3.75	0.08	0.70	7.9	11	0.74	0.0072	0.61	2.0	9.7
NGC 7160I	a	0.16	0.04	6	1.67	0.26	0.70	2.8	2.8	1.00	0.0012	0.098	2.0	5.3
NGC 7160J	a	0.33	0.04	8	2.01	0.13	0.70	3.2	7.1	0.45	0.0024	0.20	2.7	7.6
NGC 7160K	a	0.067	0.03	3	4.30	0.45	0.70	1.5	2.6	0.57	0.00049	0.041	1.0	5.6
NGC 7160L	a	0.20	0.04	7	3.23	0.21	0.70	2.1	6.4	0.33	0.0015	0.12	1.0	5.3
NGC 7160M	a	0.56	0.07	21	4.82	0.13	0.70	2.3	11	0.20	0.0041	0.34	1.1	3.0
NGC 7160N	a	0.33	0.05	11	4.97	0.16	0.70	3.7	6.6	0.56	0.0024	0.20	1.0	5.3
NGC 7160O	a	0.13	0.03	4	4.26	0.25	0.70	2.3	3.7	0.63	0.00095	0.080	0.7	3.9
NGC 7160P	a	0.21	0.04	7	4.02	0.19	0.70	2.0	5.9	0.33	0.0015	0.13	1.3	9.5
NGC 7160Q	a	0.33	0.05	12	6.04	0.16	0.70	5.5	7.7	0.71	0.0024	0.20	1.0	3.5
NGC 7160R	a	0.22	0.05	9	4.05	0.24	0.70	3.7	4.5	0.81	0.0016	0.14	1.0	3.7
NGC 7380A	a	0.73	0.05	22	5.33	0.07	3.60	34	53	0.64	0.14	12.	1.5	11.
NGC 7380B	a	0.93	0.05	20	4.62	0.06	3.60	21	63	0.33	0.18	15.	2.8	20.
NGC 7380C	a	0.38	0.04	13	4.16	0.11	3.60	20	31	0.65	0.073	6.2	1.1	4.9
NGC 7380D	a	1.7	0.06	29	5.84	0.04	3.60	36	68	0.53	0.33	28.	2.1	15.
NGC 7380E	A	0.93	0.05	22	6.91	0.06	3.60	19	75	0.25	0.18	15.	2.6	13.
NGC 7380F	L	1.6	0.11	24	2.03	0.07	<1.00	<9.3	<13	0.73	<0.025	<2.1	4.1	21.
Bk 59A	A	7.4	0.11	49	5.72	0.02	1.00	14	32	0.44	0.11	9.3	7.2	55.
Bk 59B	a	0.61	0.02	4	4.21	0.04	1.00	8.0	9.9	0.81	0.0091	0.76	3.3	24.
Bk 59C	A	23.5	0.16	144	4.18	0.01	1.00	18	54	0.34	0.35	29.	4.5	40.
Bk 59D	A	2.6	0.08	48	2.53	0.03	1.00	13	21	0.62	0.039	3.3	3.4	16.
Bk 59E	A	19.7	0.17	144	5.60	0.01	1.00	28	43	0.66	0.29	25.	5.9	40.
NGC 103A	a	0.39	0.04	9	2.62	0.11	3.03	14	37	0.37	0.053	4.5	2.7	13.
NGC 281A	A	2.7	0.08	35	2.95	0.03	2.20	28	43	0.67	0.20	16.	4.6	36.
NGC 281B	a	0.73	0.07	20	2.58	0.10	2.20	17	33	0.51	0.053	4.5	2.4	8.8
Bk 62A	a	0.59	0.04	9	4.19	0.07	2.05	17	17	1.00	0.037	3.1	2.8	17.
Bk 62B	L	0.86	0.05	24	7.72	0.06	<1.00	<13	<15	0.89	<0.013	<1.1	2.3	11.
Bk 62C	a	0.53	0.04	20	3.69	0.08	2.05	15	27	0.54	0.033	2.8	1.2	6.7
NGC 433A	a	0.44	0.03	11	4.10	0.08	4.50	34	46	0.73	0.13	11.	2.1	11.
NGC 433B	a	0.26	0.01	9	2.22	0.06	4.50	25	48	0.52	0.078	6.6	2.0	6.0
NGC 433C	a	0.36	0.03	13	2.48	0.10	4.50	25	63	0.40	0.11	9.1	1.6	6.3
NGC 433D	a	0.43	0.03	12	2.99	0.08	4.50	24	65	0.37	0.13	11.	2.2	7.9
NGC 663A	a	4.7	0.13	63	6.52	0.03	2.53	43	65	0.66	0.45	38.	3.2	26.
NGC 663B	a	0.75	0.04	17	4.38	0.06	2.13	22	33	0.68	0.051	4.3	3.4	17.
NGC 663C	a	13.4	0.16	132	4.78	0.01	2.53	62	100	0.62	1.3	110.	5.7	35.

TABLE 4—Continued

Cloud	Class	$S_{\text{CO}}$ (K km s <sup>-1</sup> )	$\sigma_{S_{\text{CO}}}$ (K km s <sup>-1</sup> )	$N$	$V_{\text{eqw}}$ (km s <sup>-1</sup> )	$\sigma_V$ (km s <sup>-1</sup> )	$d$ (kpc)	$a_{\text{min}}$ (pc)	$a_{\text{maj}}$ (pc)	$\frac{a_{\text{min}}}{a_{\text{maj}}}$	$L_{\text{CO}}$ ( $L_{\odot}$ )	$M$ ( $10^3 M_{\odot}$ )	Peak $T_{\text{R}}^*$ (K)	Peak $N(\text{H}_2)$ ( $10^{20} \text{ cm}^{-2}$ )
NGC 663D	L	0.99	0.05	25	3.07	0.06	<1.00	<7.7	<21	0.37	<0.015	<1.2	2.8	12.
NGC 663E	L	0.24	0.01	7	2.35	0.07	<1.00	<5.4	<12	0.44	<0.0036	<0.30	2.4	7.0
NGC 663F	L	0.82	0.04	16	2.32	0.06	<1.00	<7.5	<15	0.51	<0.012	<1.0	2.7	11.
NGC 663G	L	1.8	0.07	30	5.07	0.04	<1.00	<12	<25	0.49	<0.027	<2.3	3.0	22.
NGC 663H	L	1.3	0.06	23	3.73	0.05	<1.00	<8.7	<17	0.51	<0.019	<1.6	2.2	14.
Stock 5A	a	0.65	0.03	20	2.84	0.05	1.60	9.2	23	0.39	0.025	2.1	2.4	12.
Stock 5B	a	0.19	0.02	7	2.95	0.12	1.60	5.3	16	0.34	0.0073	0.61	1.0	6.3
Stock 5C	a	0.89	0.04	29	2.73	0.05	1.60	20	31	0.63	0.034	2.9	2.2	7.9
Stock 5D	a	3.7	0.08	61	5.18	0.02	1.60	22	48	0.46	0.14	12.	2.6	17.
Stock 5E	a	0.24	0.03	8	1.87	0.13	1.60	9.5	11	0.87	0.0092	0.77	2.2	5.8
Stock 5F	a	0.15	0.02	5	2.72	0.14	1.60	6.4	8.7	0.74	0.0058	0.48	2.0	8.6
Stock 5G	a	0.27	0.03	9	2.41	0.12	1.60	8.1	13	0.62	0.010	0.87	1.7	7.0
Stock 5H	a	3.1	0.06	56	1.78	0.02	1.60	14	42	0.33	0.12	10.	6.5	19.
Stock 5I	a	3.9	0.07	73	1.93	0.02	1.60	29	43	0.68	0.15	13.	5.1	13.
NGC 744A	a	0.10	0.02	4	2.53	0.22	1.50	5.5	6.0	0.91	0.0034	0.28	1.3	5.3
NGC 744B	a	1.2	0.06	32	4.57	0.05	1.50	14	31	0.45	0.040	3.4	2.2	17.
NGC 744C	a	0.58	0.05	19	4.74	0.10	1.50	8.4	26	0.32	0.019	1.6	1.3	8.1
NGC 744D	a	0.49	0.04	14	3.85	0.09	1.50	11	14	0.80	0.016	1.4	1.6	9.7
NGC 957A	L	6.6	0.14	96	4.11	0.02	<1.00	<20	<27	0.75	<0.098	<8.3	3.7	29.
IC 1848A	A	9.9	0.13	76	6.20	0.01	2.31	34	63	0.54	0.79	66.	7.0	67.
IC 1848B	A	2.3	0.06	21	3.86	0.03	2.31	18	31	0.56	0.18	15.	7.9	54.
IC 1848C	A	0.35	0.02	8	3.00	0.06	2.31	12	17	0.67	0.028	2.3	2.6	12.
IC 1848D	L	0.51	0.03	8	3.11	0.07	<1.00	<4.5	<11	0.39	<0.0076	<0.64	4.0	15.
IC 1848E	A	0.28	0.05	8	3.97	0.19	2.31	12	19	0.64	0.022	1.9	1.0	5.3
IC 1848F	L	0.14	0.02	4	2.68	0.16	<1.00	<5.2	<5.2	1.00	<0.0021	<0.18	1.8	6.3
IC 1848G	a	0.23	0.04	8	3.38	0.27	2.31	6.0	24	0.25	0.018	1.5	0.9	3.5
NGC 1444A	U	0.34	0.02	9	2.55	0.07	1.00	6.1	6.8	0.90	0.0051	0.43	2.2	10.
NGC 1444B	a	0.57	0.03	15	2.30	0.06	1.00	7.7	9.8	0.79	0.0085	0.71	3.2	12.
NGC 1444C	L	0.21	0.03	9	2.08	0.15	<1.00	<4.2	<4.5	0.92	<0.0031	<0.26	2.3	10.
NGC 1444D	L	1.6	0.06	26	3.12	0.04	<1.00	<9.9	<13	0.74	<0.024	<2.0	4.9	27.
NGC 1444E	L	2.9	0.06	28	3.90	0.02	<1.00	<9.3	<22	0.42	<0.043	<3.6	4.9	31.
NGC 1444F	L	0.61	0.03	9	6.01	0.05	<1.00	<5.6	<8.7	0.64	<0.0091	<0.76	3.0	22.
NGC 1444G	U	1.3	0.06	26	4.61	0.05	1.00	7.5	14	0.54	0.019	1.6	3.7	17.
NGC 1444H	U	7.4	0.11	74	5.30	0.02	1.00	15	31	0.50	0.11	9.3	7.1	37.
NGC 1444I	L	0.27	0.02	8	1.90	0.09	<1.00	<5.8	<8.2	0.70	<0.0040	<0.34	2.2	9.5
NGC 1444J	L	2.8	0.06	62	2.58	0.02	<1.00	<13	<25	0.52	<0.042	<3.5	4.1	14.
NGC 1444K	a	0.58	0.03	18	2.60	0.06	1.00	7.0	14	0.49	0.0086	0.73	2.2	9.3
NGC 1444L	a	0.27	0.02	10	3.68	0.09	1.00	4.4	8.9	0.49	0.0040	0.34	1.2	7.0
NGC 1624A	U	0.47	0.04	10	5.88	0.09	6.00	46	62	0.75	0.25	21.	2.0	12.
NGC 1624B	A	0.70	0.05	16	4.47	0.08	6.00	38	81	0.47	0.38	32.	2.0	13.
NGC 1624C	L	0.71	0.03	12	2.71	0.05	0.30	1.7	2.8	0.59	0.00095	0.080	3.9	17.
NGC 1624D	L	3.6	0.06	35	3.62	0.02	0.30	2.4	6.1	0.39	0.0048	0.41	5.6	35.
Bk 11A	a	1.2	0.06	22	5.00	0.05	2.20	20	35	0.56	0.087	7.3	3.4	15.
Bk 11B	a	2.2	0.08	37	4.51	0.04	2.20	24	47	0.51	0.16	13.	3.0	20.
Bk 11C	a	0.13	0.01	7	1.75	0.09	2.20	5.4	15	0.37	0.0094	0.79	2.1	6.0
Bk 11D	L	0.70	0.06	15	3.44	0.09	0.80	8.7	15	0.56	0.0067	0.56	2.2	15.
Bk 11E	L	0.37	0.04	10	1.78	0.12	0.30	1.2	3.6	0.33	0.00050	0.042	2.7	8.3
Bk 11F	a	0.25	0.04	10	2.50	0.17	2.20	10	13	0.74	0.018	1.5	1.5	5.8
Bk 11G	a	0.25	0.05	9	1.57	0.21	2.20	8.1	9.6	0.84	0.018	1.5	1.7	5.8
NGC 1605A	a	1.4	0.06	27	3.56	0.05	2.72	27	49	0.54	0.15	13.	2.9	11.
NGC 1605B	L	0.27	0.02	6	3.65	0.08	0.30	2.0	2.6	0.78	0.00036	0.030	2.0	11.
NGC 1778A	L	1.1	0.05	19	3.39	0.05	0.80	7.3	13	0.58	0.011	0.88	3.3	16.
NGC 1778B	L	0.71	0.04	18	1.48	0.06	0.80	10	13	0.77	0.0068	0.57	1.8	10.
NGC 1778C	L	2.0	0.06	33	4.07	0.03	0.80	9.5	22	0.44	0.019	1.6	3.2	17.
NGC 1778D	L	0.21	0.04	8	1.47	0.20	0.30	1.3	2.0	0.66	0.00029	0.024	1.7	4.6
NGC 1893A	A	1.8	0.07	37	4.34	0.04	4.00	40	105	0.38	0.43	36.	3.3	16.
NGC 1893B	a	0.09	0.02	3	2.68	0.23	4.00	11	17	0.60	0.022	1.8	1.1	5.1
NGC 1893C	a	0.28	0.03	9	2.39	0.12	4.00	15	31	0.47	0.067	5.6	1.2	4.4
NGC 1893D	a	0.24	0.03	7	2.00	0.14	4.00	25	35	0.72	0.057	4.8	2.3	8.1
NGC 1893E	a	0.26	0.03	7	4.69	0.12	4.00	17	38	0.46	0.062	5.2	1.2	7.2
NGC 1931A	a	0.35	0.02	8	4.13	0.06	1.80	8.2	21	0.39	0.017	1.4	2.7	13.
NGC 1931B	U	0.51	0.03	12	3.79	0.07	2.30	14	25	0.56	0.040	3.4	3.0	14.
NGC 1931C	A	1.7	0.05	25	3.48	0.03	1.80	13	37	0.35	0.082	6.9	5.0	28.
NGC 2129A	a	2.4	0.06	33	5.02	0.03	2.00	27	33	0.84	0.14	12.	2.8	20.
NGC 2129B	a	0.44	0.03	13	4.04	0.07	2.00	13	23	0.54	0.026	2.2	1.7	7.2
NGC 2129C	a	1.6	0.04	33	3.42	0.03	2.00	21	46	0.46	0.095	8.0	2.9	13.
NGC 2175A	U	15.5	0.13	58	7.18	0.01	3.50	70	79	0.88	2.8	240.	6.2	78.
NGC 2175B <sup>a</sup>	A	27.1	0.15	85	6.04	0.002	1.95	35	55	0.64	1.5	130.	13.4	140.
NGC 2175C	a	2.1	0.07	17	3.99	0.05	1.95	11	25	0.43	0.12	10.	2.9	24.
NGC 2175D	a	0.21	0.02	6	3.12	0.11	1.95	13	20	0.62	0.012	1.0	2.0	8.3
NGC 2175E	a	0.72	0.03	15	2.39	0.05	1.95	13	32	0.39	0.041	3.4	2.0	7.2
NGC 2175F	L	1.3	0.05	29	3.77	0.04	<1.00	<5.4	<23	0.24	<0.019	<1.6	3.3	13.
NGC 2175G	A	14.3	0.15	101	6.32	0.01	1.95	36	68	0.53	0.81	68.	6.3	51.
Monoceros A	A	4.9	0.10	51	6.06	0.02	2.40	19	42	0.45	0.42	35.	5.9	54.

<sup>a</sup> Due to the misplacement of a decimal point by the author, the CO flux, luminosity, and mass of cloud NGC 2175B appear incorrectly (a factor of 10 too high) in Paper I.

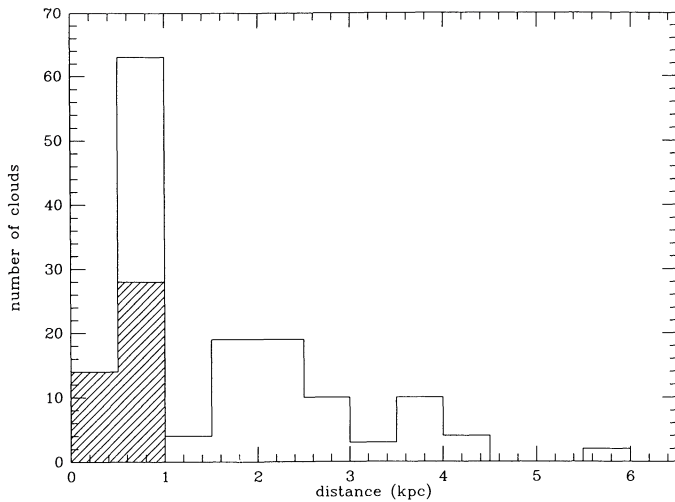


FIG. 1a

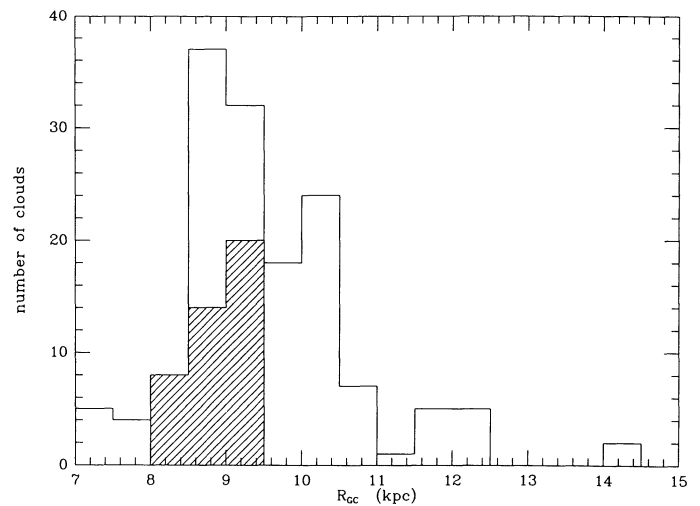


FIG. 1b

FIG. 1.—Histograms of (a) heliocentric and (b) galactocentric distances of cataloged molecular clouds. Hatched area describes local dark clouds.

classification. Clouds of class *A* are at the well-known distances of the stars with which they are associated (Leisawitz 1988, and references therein). Likewise for clouds of class *U*. The distances of local dark clouds, in many cases, are known from star counting or by association with relatively nearby stars (see Paper I, and references therein); 1 kpc upper limits are adopted for these clouds in the absence of substantial information. Clouds of class *a* are assumed to lie at the distances of the clusters near which they are found. If, instead of being associated with the clusters, these latter clouds were more distant than the clusters, the clouds would in many cases be offset from the Galactic midplane by an amount that is large relative to the molecular cloud scale height ( $\sim 150$  pc FWHM in the outer Galaxy); thus, class *a* clouds that are, in fact, not associated with the surveyed clusters are more likely than not to be closer than the clusters (see § Va).

Table 4 contains physical properties of the clouds: CO line flux (eq. [1]), the number of lines of sight,  $N$ , toward which emission from the cloud was detected, CO line width (eq. [7]), distance, major and minor axis lengths in parsecs, CO line luminosity (eq. [2]), cloud mass (eq. [4]), and the peak values of  $T_R^*$  and  $H_2$  column density (eq. [3]) found in the cloud. The ratio  $a_{\min}/a_{\max}$  is given as an estimator of the nonsphericity of the cloud; although clouds with  $a_{\min}/a_{\max} \sim 1$  may be nonspherical, clouds with  $a_{\min}/a_{\max} \ll 1$  clearly are nonspherical.

#### b) Overview of the Properties of Cataloged Clouds

Using the tabulated data, let us take a first look at the contents of the catalog. Cloud distance information is summarized in Figure 1. Most of the clouds at  $d < 1$  kpc are local dark clouds (shaded histograms). The clouds are confined to a narrow range of galactocentric distance, since the local clouds are at the solar circle ( $R_{GC} = 8.5$  kpc), and most of the surveyed open clusters are in the Perseus arm just outside the solar circle (see Fig. 3c in Paper I). The survey coverage was concentrated around the Galactic plane, primarily in the second quadrant of Galactic longitude.

In Figures 2 and 3 are cumulative frequency distributions of cloud radius and mass. Observational selection effects, discussed below in § IIIc, limit the range of cloud sizes. As cloud mass scales in some way with cloud size (see § IVb), the selec-

tion effects that truncate the size distribution similarly influence the mass distribution. A line fit by eye to the cloud size distribution in the range in which observational selection effects are unimportant has a slope about  $-1.6$  (i.e.,  $N[R > R_0] \propto R_0^{-1.6}$ ). Terebey *et al.* (1986) derived effectively the same slope ( $-1.6_{-0.7}^{+1.9}$ ) from a sophisticated analysis of a relatively small sample of clouds and discussed how systematic biases may have affected earlier derivations of the molecular cloud size spectrum. From Figure 3, we find  $N(M > M_0) \propto M_0^{-0.65}$ , which agrees well with previous determinations of the cloud mass spectrum (see, e.g., Casoli, Combes, and Gerin 1984, and references therein).

Following tradition, mean cloud densities are computed from the masses and radii assuming spherical geometry. From

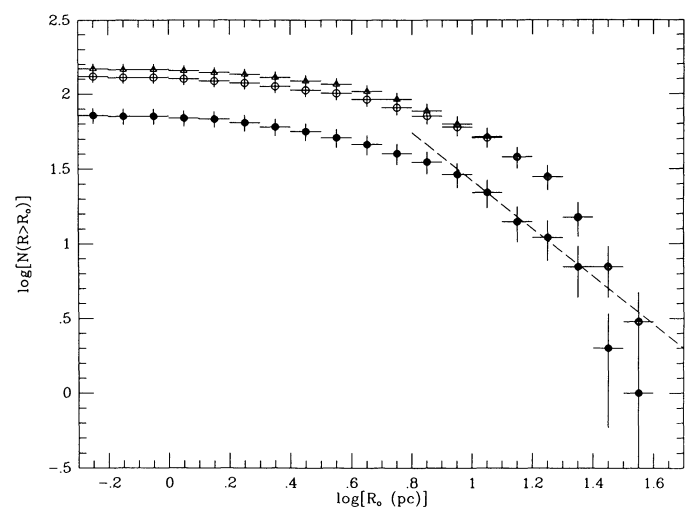


FIG. 2.—The number of clouds with radius bigger than  $R_0$  as a function of  $R_0$ . Completely mapped clouds with measured distances are shown with filled circles, all clouds (including those not completely mapped) with measured distances are shown with open circles, and all cataloged clouds (including 17 with distance upper limits) are shown with triangles. Horizontal “error bars” show bin widths, and vertical error bars represent the sample statistics. The dashed line is a fit by eye to the data and has slope  $-1.6$ . As expected, the slope is steeper in the samples that include incompletely mapped clouds.

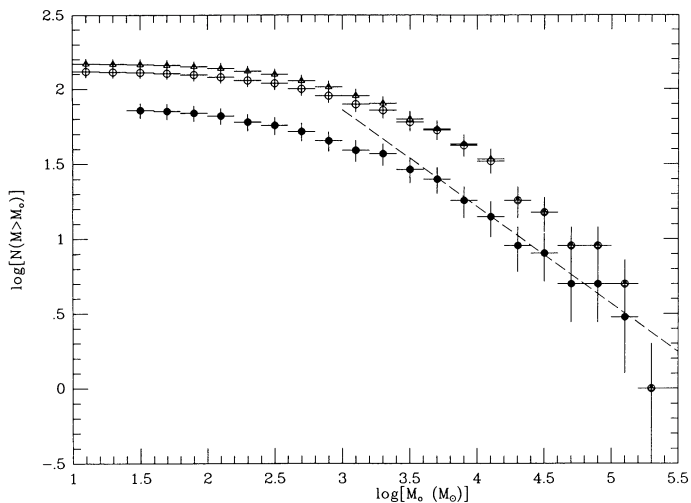


FIG. 3.—The number of clouds with mass greater than  $M_0$  as a function of  $M_0$ . Symbols are the same as in Fig. 2. The dashed line has slope  $-0.65$ .

the histogram shown in Figure 4, it appears that cataloged clouds range in density from about  $10\text{--}10^3$   $\text{H}_2$  molecules per  $\text{cm}^3$ . In § IVb, where errors in cloud distance are properly considered, it is shown that the actual range of densities is much smaller and that a typical mean density is about  $20$   $\text{H}_2$   $\text{cm}^{-3}$ .

For excitation of the CO  $J = 1 \rightarrow 0$  line to be dominated by  $\text{H}_2\text{--CO}$  collisions, as it is customary to assume, the  $\text{H}_2$  density in line-emitting regions has to exceed a critical value about  $10^3$   $\text{cm}^{-3}$ . Since the typical observed mean cloud density is much lower than the critical density, it follows that the CO emitting regions should fill a small fraction of the cloud volume, a notion that turns out to be consistent with other millimeter observations of molecular clouds (see below).

The CO line widths of a large majority of the cataloged clouds range from about  $2.5$  to  $6$   $\text{km s}^{-1}$  (Fig. 5). The line width distribution is reminiscent of the one found for small

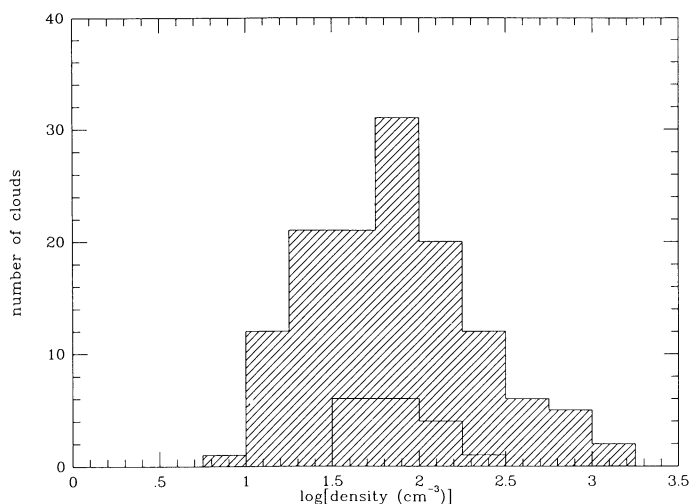


FIG. 4.—Histograms of the mean volume density of  $\text{H}_2$  molecules in cataloged clouds. The upper histogram represents clouds with measured distances. The lower one represents the 17 local dark clouds with distance upper limits and therefore shows lower limits in density. Due to measurement errors, the density dispersion implied by the depicted distribution grossly overestimates the actual spread of cloud densities (see text).

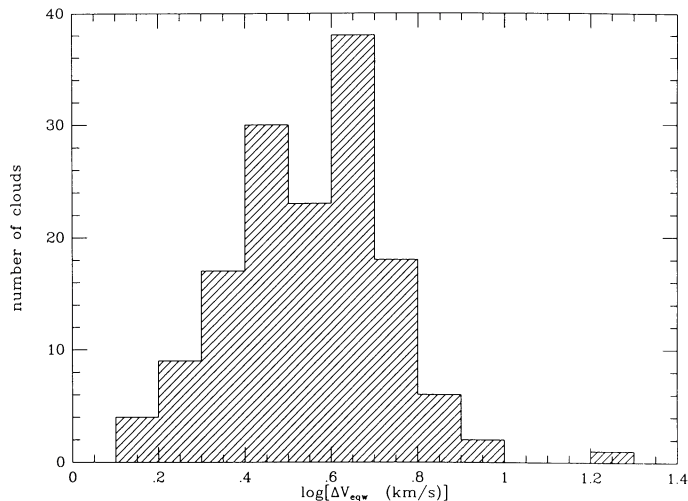


FIG. 5.—Distribution of the CO line equivalent widths (eq. [7]) of cataloged clouds derived from their composite spectral line profiles.

dark clouds by Clemens and Barvainis (1988), or of the distribution found for massive clouds in the outer Galaxy by Mead and Kutner (1988). Note that the survey contains relatively few clouds of broad line width as found in the CO surveys of the inner Galaxy (Sanders, Scoville, and Solomon 1985; Solomon *et al.* 1987; Dame *et al.* 1986). Because of their limited spatial resolution or undersampling, the inner Galaxy surveys are most sensitive to clouds more massive than  $10^4 M_\odot$ , clouds which tend to have the widest CO lines (see § IV).

Figure 6 shows the distribution of peak antenna temperatures ( $T_A^*$ ) detected in the cataloged clouds. Most of the clouds have a peak  $T_A^*$  in the range  $1\text{--}5$  K. If the CO  $J = 1 \rightarrow 0$  line emission comes from regions that are optically thick at the line rest frequency, and the CO in these regions is collisionally excited,  $T_R^* (= T_A^*/0.82)$  should be an approximate measure of the gas kinetic temperature,  $T_k$ , for a cloud that uniformly illuminates the telescope beam. In this naive interpretation, the observed range in peak  $T_A^*$  corresponds to  $4 \text{ K} < T_k < 9 \text{ K}$ , in agreement with the outer Galaxy cloud envelope temperature reported by Mead and Kutner (1988).

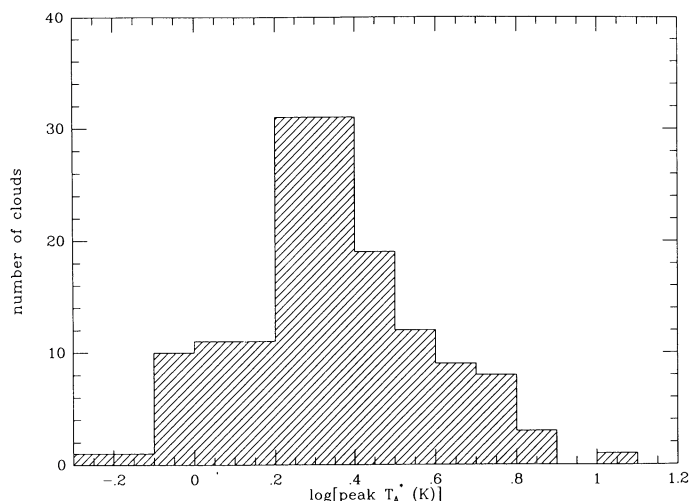


FIG. 6.—Distribution of the maximum CO antenna temperatures found in cataloged clouds.

The temperatures of molecular clouds have been probed in a variety of ways. A history of observations made with numerous telescopes and degrees of spatial resolution, employed to measure the level populations of, e.g., CO, NH<sub>3</sub>, and CH<sub>3</sub>OH in molecular clouds, leads to the reasonably secure conclusion that cloud kinetic temperatures typically range from 10–20 K and sometimes are greater (Evans 1980; Goldsmith 1987). Similar temperatures are commonly measured for the dust in molecular clouds from their far-infrared spectra (see, e.g., Wu and Evans 1989). The fact that we measure antenna temperatures an order of magnitude lower than typical molecular cloud kinetic temperatures probably indicates that the emitting regions are clumps of molecular gas (Blitz and Shu 1980; Zuckerman and Evans 1974) that do *not* uniformly fill the Columbia-GISS telescope's 8.7 beam. Alternatively, it is possible that the CO line is radiatively, not collisionally, excited, or that it is not optically thick as assumed, but it would then be difficult to account for the preponderance of observations from which kinetic temperatures greater than or equal to 10 K are derived.

Thus, two observations, which are not strictly independent, seem to imply that molecular clouds are ensembles of CO-emitting clumps: (1) the cloud mean densities are much lower than the critical density required to excite CO molecules collisionally, and (2) the measured antenna temperatures are much lower than the typical gas kinetic temperature. In this interpretation, each clump has an extremely narrow thermal line width ( $\sim 0.1 \text{ km s}^{-1}$  FWHM) compared to the measured CO line width of the cloud (Fig. 5), and the cloud line width is assumed to measure the velocity dispersion of the clumps. Observation (1) implies that the clumps fill a small fraction of the cloud volume, while observation (2) implies that the total projected surface area of the clumps *at a given radial velocity* is less than the projected area of the cloud. The overall surface filling fraction of clumps must not be less than one, however, for otherwise, contrary to their appearance on the Palomar Sky Survey prints, molecular clouds would be full of holes.

If beam dilution explains why  $T_A^*$  is much less than  $T_k$ , then it is possible to estimate the beam filling fraction of the CO-emitting clumps and to place an upper limit on their size from the area illuminated by the beam at the distance of the cloud. The greatest  $T_R^*$  recorded in the local dark cloud NGC 6694E, for example, is 2.0 K. Even if the kinetic temperature is only 10 K, the beam filling fraction must not exceed 0.3 in any of the 33 observed positions in the cloud. At the distance of NGC 6694E, 0.2 pc, the beam diameter is 0.5 pc. Hence, if the 2 K spectral line is produced by a single clump, the clump diameter is 0.3 pc (see Falgarone and Puget 1985, and references therein). Still tighter constraints have been placed on the clump sizes in molecular clouds by observations of local clouds made with large millimeter telescopes (Falgarone and Péreault 1988; also see Myers and Benson 1983).

A virtue of the clumpy cloud model is its ability to account for empirical evidence that the intensity of the optically thick CO line probes the column density of a molecular cloud (eq. [3]). Consider, in support of this relation, that the molecular cloud mass derived from an LTE analysis using observations of the optically thin <sup>13</sup>CO  $J = 1 \rightarrow 0$  line is in reasonable agreement with the mass calculated from <sup>12</sup>CO observations (see, e.g., Dame 1983; Lee, Snell, and Dickman 1990). Also, the <sup>12</sup>CO line intensity has been found to correlate with blue extinction (see, e.g., Leisawitz and Klingensmith 1989) and with the gamma-ray intensity observed toward molecular clouds

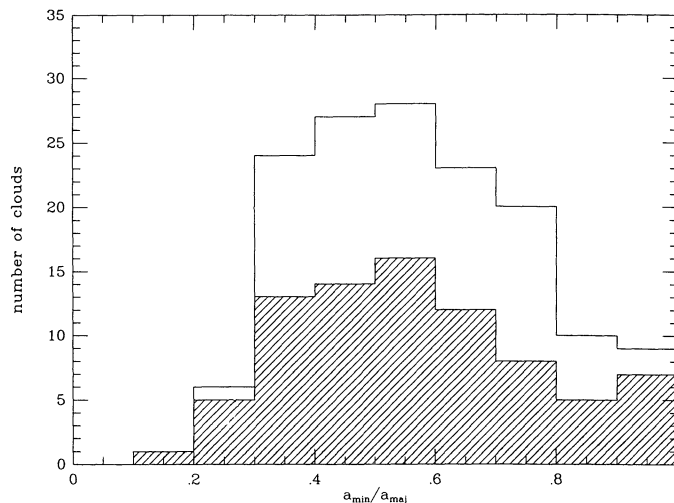


FIG. 7.—Distributions of the minor-to-major axis ratios of all cataloged clouds (*upper histogram*) and those that were mapped completely (*lower histogram*) showing that the clouds are not spherical.

(Bloemen *et al.* 1984), both of which, presumably, are proportional to the H<sub>2</sub> column density. If in a given line of sight the clumps of CO-emitting gas are spread out in velocity with a dispersion greater than the thermal line width of a clump, the line intensity is a measure of the number of clumps in the beam and hence of the total molecular column density (see, e.g., Dickman, Snell, and Schloerb 1986).

Molecular clouds found in the open cluster survey are distinctly nonspherical. This is evident in the histogram of axis ratios,  $a_{\min}/a_{\max}$ , shown in Figure 7. The expected axis ratio distribution for a population of clouds that are essentially spherical but with surface irregularities peaks at  $a_{\min}/a_{\max} = 1$  and falls rapidly to zero at the ratio characteristic of the maximum distortion (Leisawitz 1985). The dark clouds discussed by Clemens and Barvainis (1988) also were shown to be nonspherical. David and Verschueren (1987) analyzed the shapes of clouds in our catalog in some detail and found that, while the local dark clouds are distributed in  $a_{\min}/a_{\max}$  in a manner consistent with uncorrelated axis lengths, the clouds that are (or may be) associated with clusters have a more well-defined shape, are definitely not oblate, and may be prolate.

Since the clouds are noncircular in projection, one might ask whether their major axes are aligned in any special way with respect to the Galactic plane. Figure 8 shows the frequency distribution of major axis Galactic position angles from Table 3. Clearly there is no preferred orientation; the angles appear to be distributed randomly to the extent that can be determined given the Poisson counting errors. On the other hand, to zeroth order, the Galactic magnetic field is circular, and the field lines are parallel to the Galactic plane (Heiles 1987, and references therein). Although these observations suggest that the molecular clouds are not strongly coupled to the large-scale magnetic field, the field fluctuates on smaller scales, and it cannot be dismissed without further investigation as having no influence on the cataloged clouds.

#### c) Bias and Completeness in the Cloud Catalog

In general, a CO survey can be limited in completeness in terms of both the sizes and the densities of molecular clouds

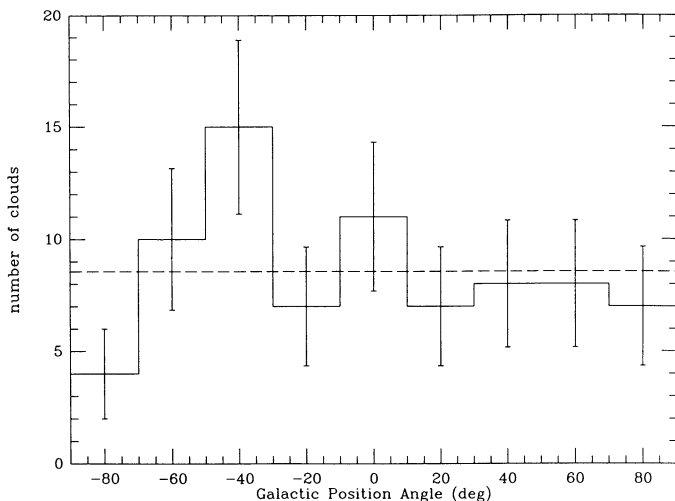


FIG. 8.—Position angles of cloud major axes with respect to the Galactic plane. Only those (77) clouds that were mapped completely and for which  $a_{\min} \neq a_{\max}$  are shown. Error bars show statistical uncertainties. The dashed line illustrates the mean number of clouds per bin expected if the clouds are randomly oriented.

that can be found. The present survey, however, was designed to enable detection of even the most tenuous clouds. A resolved cloud through which the column density of  $H_2$  molecules is as low as  $2 \times 10^{20} \text{ cm}^{-2}$  should produce a detectable CO line. For a normal ratio of dust to gas, about 0.01 by mass, this column density corresponds to a  $1000 \text{ \AA}$  optical depth  $\sim 0.9$  (Savage and Mathis 1979, and references therein). Since UV photons of the general interstellar radiation field are capable of dissociating  $H_2$  molecules, it is safe to assume that few, if any, molecular clouds have column densities lower than those to which the present survey is sensitive.

Clouds that are small in angular extent are not cataloged, and maps of clouds that subtend large solid angles tend to be incomplete. To be specific, as a result of the telescope beam size and survey sampling interval, clouds smaller than about  $10'$

will be overlooked; smaller clouds can be detected, and indeed they are, but they are not cataloged (see § II). All larger clouds in the surveyed regions are resolved, detected, and cataloged. At 1 kpc, the distance of the most remote “local cloud,” a cloud as small as  $\sim 3 \text{ pc}$  in diameter, can be resolved; at the distance of the most remote cluster in our survey, an 18 pc diameter cloud can be resolved. Because unresolved sources suffer beam dilution and produce weak signals in isolated positions, they are difficult to count. Fourteen possible unresolved sources, approximately  $4 \text{ deg}^{-2}$ , are located in the region surveyed around NGC 1893, centered at  $l = 173^\circ.6$ ,  $b = -1^\circ.7$ .

Due to the limited coverage of the survey (see Table 2), clouds of large angular extent,  $\sim 1^\circ$  or larger, tend to be mapped incompletely. In most cases, complete low-resolution maps of such large clouds can be found in the Columbia-GISS CO survey of the Galactic plane (Dame *et al.* 1987). Frequency distributions of the angular sizes and mean CO intensities ( $\langle I_{\text{CO}} \rangle = S_{\text{CO}}/N$ ) of cataloged clouds are shown, respectively, in Figures 9 and 10. For comparison, analogous distributions are shown for those of our clouds that were mapped completely and those that also were found in the Galactic plane survey. Although the open cluster survey and the Galactic plane survey can be seen to differ in their sensitivity to faint sources and to clouds of small angular extent, clouds brighter than  $8 \text{ K km s}^{-1}$  and more extended than  $1^\circ$  in diameter are seen about equally well by both surveys.

As noted earlier, the cataloged clouds were classified according to whether they are conclusively (*A*) or possibly (*a*) associated with open clusters, are local dark clouds (*L*), or are other known regions of star formation (*U*). Clouds of one class were found to differ in some ways from clouds of other classes, but most of the differences are attributable to selection effects. For example (see § Vc), class *L* clouds are smaller and less massive than average. This is at least in part a consequence of the different cloud size completeness limits that pertain to local versus nonlocal clouds as a result of a fixed survey resolution and limited coverage. It is well known (see, e.g., Dame and Thaddeus 1985) that *some* local molecular clouds are both large ( $R > 25 \text{ pc}$ ) and massive ( $> 10^5 M_\odot$ ), but physically large

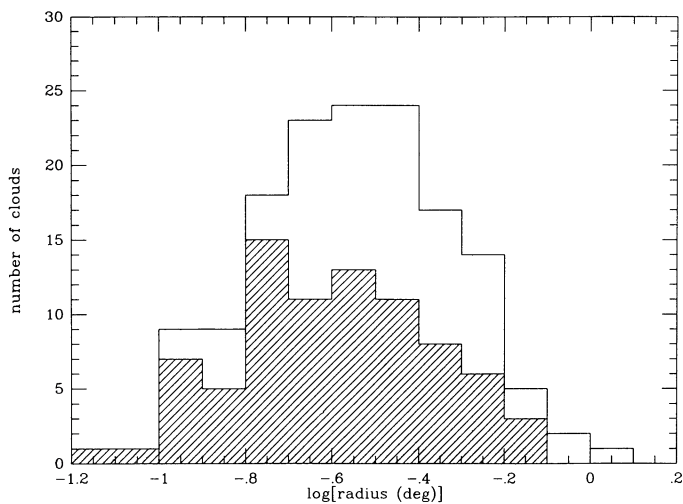


FIG. 9a

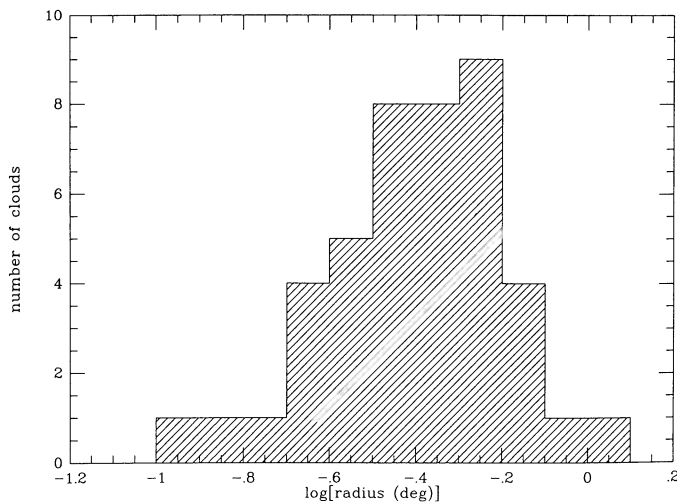


FIG. 9b

FIG. 9.—Distributions of cloud angular radii. In (a) the upper histogram represents all clouds in the catalog and the hatched histogram shows the completely mapped clouds; the histogram in (b) pertains to cataloged clouds that were seen in the Columbia CO survey of the Galactic plane. Note that the latter clouds subtend relatively large angles.

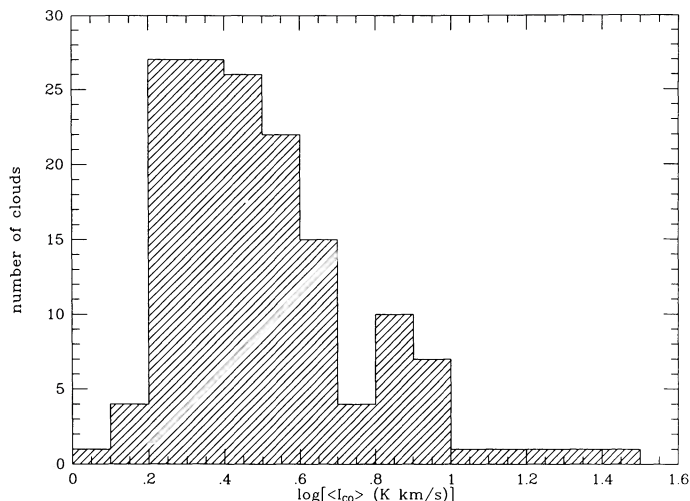


FIG. 10a

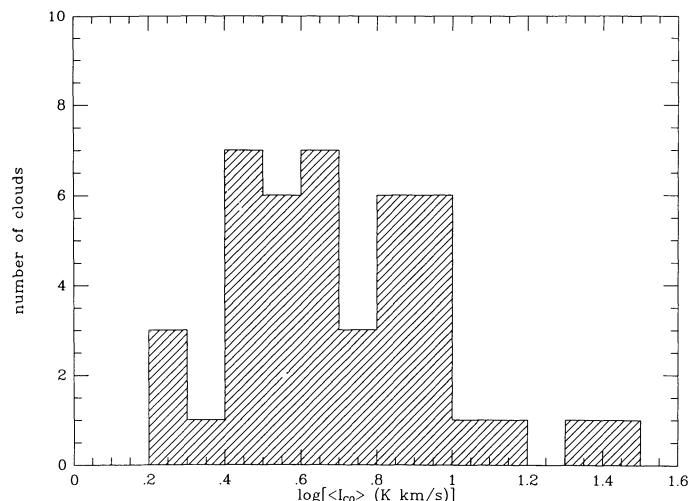


FIG. 10b

FIG. 10.—Mean CO intensities ( $\int T_R^* dv$ ) of (a) all clouds in catalog and (b) those clouds that were seen in the Columbia CO survey of the Galactic plane. Few clouds in the latter survey have a mean line intensity less than about  $3 \text{ K km s}^{-1}$ .

clouds are large in angular extent and tend not to be completely mapped in the cluster survey. Mean sizes and masses of clouds of different classes are shown in Table 5.

Samples of clouds divided by class also differ in their distributions of mean CO intensity, but again selection effects can account for the observed differences. First consider classes *A* and *a*, all the clouds that are, or may be, associated with young open clusters. Clouds of class *a* tend to be weak sources of CO emission, whereas class *A* clouds are all strong CO sources (see Fig. 11). The hypothesis that class *A* clouds are distributed in  $\langle I_{\text{CO}} \rangle$  in the same way as class *a* clouds can be rejected at a level of confidence greater than 99% (from a  $\chi^2$  analysis). This segregation may be related to the primary criterion used to classify a cloud as type *A* rather than *a*: a bright rim on the cloud surface, indicating its interaction with the H II region ionized by a cluster, is a necessary condition for membership in class *A*. One might expect to find a relatively high emission measure at the ionized surface of a cloud that is relatively high in CO column density, since both observables depend on the line-of-sight path length through the cloud. If so, then clouds with high mean CO intensity are more likely than clouds with low CO intensity to have bright rims and to be assigned to class *A*. Furthermore, class *A* clouds appear to be relatively warm (see § Vc).

Yet another selection effect accounts for the paucity of weak CO sources in the local cloud sample (Fig. 11, *bottom*). The

visual extinction produced by dust in a molecular cloud with a mean CO line intensity less than  $2 \text{ K km s}^{-1}$  is so low ( $\sim 0.4$  mag; Savage and Mathis 1979) that the cloud will hardly attenuate the visible star density in its direction. Clouds were classified as type *L* only if, in addition to having LSR velocities near zero, they were found to correspond to heavily obscured regions on the POSS prints; clouds that were not considered to satisfy both conditions were classified as type *a*, since it could not be ruled out that they are associated with an open cluster. Except for the lack of weak CO clouds in the local cloud sample, the mean CO intensities of local clouds do not differ significantly from those of class *a* clouds.

#### IV. EMPIRICAL SCALING RELATIONS AND THEIR SIGNIFICANCE

Line width–size and density–size scaling relations have been widely reported for molecular clouds (see, e.g., Larson 1981, and recent reviews by Myers 1987 and Scalo 1987). The form of these relations, and indeed the fact that they exist at all, tells us something interesting about the physical nature of the clouds. Line width–size and density–size relations are derived in §§ IVa and IVb for the cataloged clouds. In § IVc we show that the clouds are not in virial equilibrium; in particular, the clouds may be ensembles of CO-emitting clumps, but the clump-clump velocity dispersion is always too large for the cloud gravity if the cloud is in equilibrium. We offer a possible explanation for the observations in § IVd.

TABLE 5  
SIZES AND MASSES OF CLOUDS SORTED BY CLASS

CLASS	NUMBER IN SAMPLE	RADIUS (pc)			MASS ( $M_{\odot}$ )		
		$\langle \log R \rangle$	$\sigma_{\log R}$	Median $\log R$	$\langle \log M \rangle$	$\sigma_{\log M}$	Median $\log M$
A .....	20	1.14	0.23	1.15	4.17	0.58	4.20
a .....	77	0.85	0.37	0.87	3.31	0.79	3.30
L <sup>a</sup> .....	25	0.34	0.34	0.28	2.37	0.65	2.50
U .....	9	1.05	0.35	1.00	3.86	0.77	3.85
Total <sup>a</sup> .....	131	0.81	0.43	0.85	3.30	0.91	3.30

<sup>a</sup> The 17 local dark clouds with unknown distances are excluded.

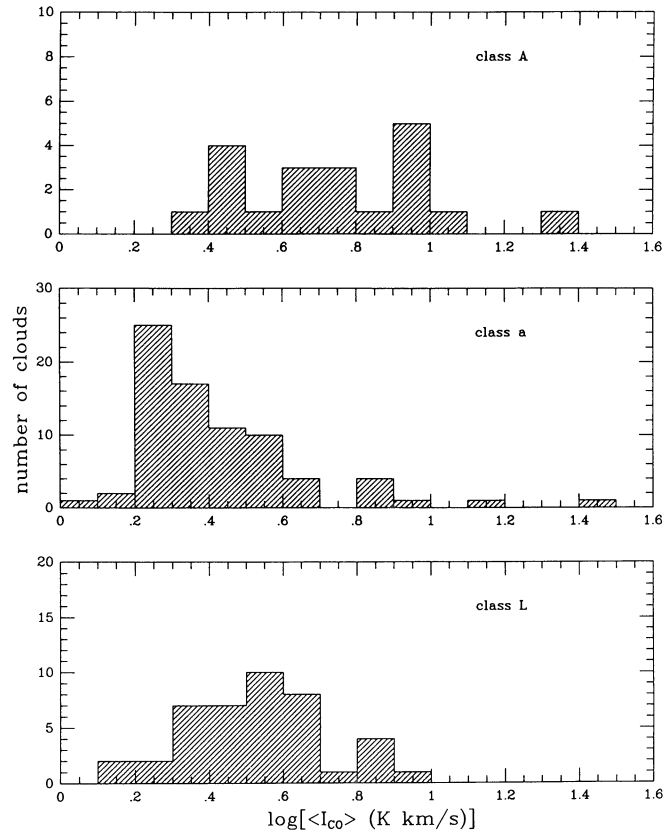


FIG. 11.—Mean CO intensities ( $\int T_R^* dv$ ) of clouds sorted by class. Clouds in class A (those known to be associated with extremely young open clusters) tend to be brighter than the other clouds.

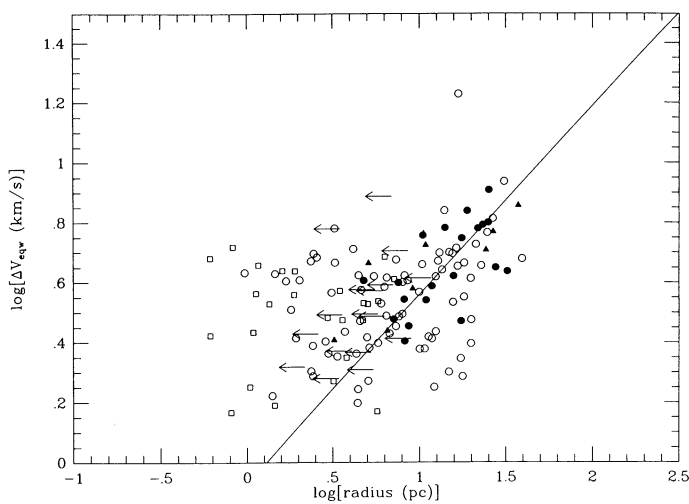


FIG. 12a

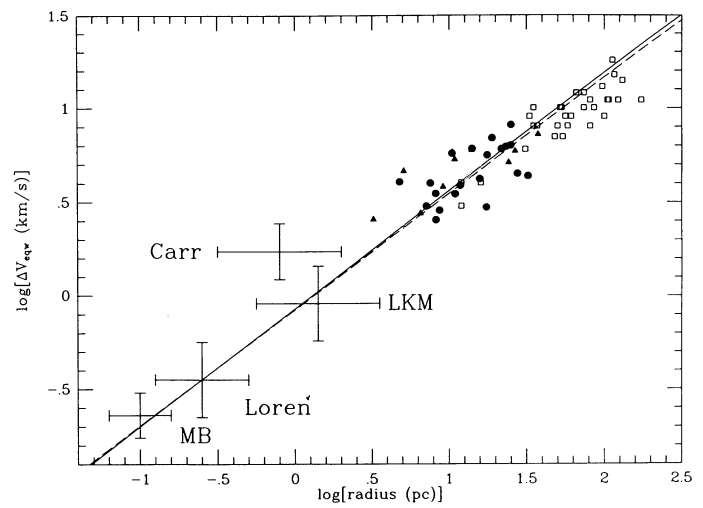


FIG. 12b

FIG. 12.—Mean CO line equivalent widths and radii of molecular clouds. In (a), cataloged clouds are represented with different symbols for different cloud classes: filled circles for class A, open circles for class a, filled triangles for class U, and open squares for class L. Arrows represent class L clouds with distance upper limits. Filled symbols are reserved for clouds with relatively well-known distances. Class A and class U clouds are shown again in (b) along with the large molecular cloud complexes of Dame *et al.* (1986; squares). Also shown with “error bars” in (b) are ranges of CO line width and cloud size for the clouds studied by Leung, Kutner, and Mead (1982, LKM), Myers and Benson (1983, MB), Carr (1988), and Loren (1988b). In (a) and (b), the solid line is described by eq. (8) with the mean parameters given in the text. For comparison, the dashed line in (b) is a least-squares fit to the class A, class U, and Dame *et al.* clouds only (see Table 6A).

### a) The Line Width–Size Relation

Figure 12a shows the linewidths and sizes of molecular clouds found in the open cluster CO survey. The large scatter, especially in the points that represent small clouds, can be attributed to errors in both size and line width. Small clouds tend to have poorly determined sizes because most of them are local dark clouds or clouds whose association with a cluster is not firmly established and, in either case, the cloud distance is not known accurately or with confidence; the fractional error in cloud angular size also can be appreciable. For small clouds, which tend not to be well resolved, the fractional uncertainty in line width is inversely proportional to the square root of the number of observed positions. The line widths and sizes of class A and class U clouds, which have relatively well-known distances, are shown in Figure 12b. The giant molecular cloud complexes cataloged by Dame *et al.* (1986) are also represented in this figure and can be seen to extend a trend in which the CO line widths and sizes of molecular clouds are related by a power law. The cross hairs in Figure 12b symbolize the ranges of cloud size and line width in other published data sets with which the cluster survey data will be compared.

A numerical nonlinear least-squares method (Jeffreys 1980) was used, the objective of which was to minimize the weighted sum of squared errors with errors in both line width and cloud size taken into account. Analyses of various samples of clouds were done to check for undesirable variation of the best-fit parameters. These “trial” fits are of the general form

$$\log(\Delta V_{\text{eqw}}) = a_1 \log R + a_2, \quad (8)$$

and the results are shown in Table 6A. Appropriate distance errors were assigned to estimate the size uncertainty of each cloud (see footnote to Table 6). Mean parameter values based on the trial fits weighted by their associated formal errors are  $a_1 = 0.63 \pm 0.05$  and  $a_2 = -0.071 \pm 0.067$ . The errors assigned to these parameters are worst-case errors derived assuming the individual trials are not independent. Parameters derived

TABLE 6  
EMPIRICAL LINE WIDTH-SIZE RELATIONS<sup>a</sup>

Cloud Sample	Number of Clouds	$a_1^b$	$a_2^b$	rms Residual	Notes	References
A. This Paper						
Classes <i>A</i> and <i>U</i> .....	29	0.97 (0.24)	-0.45 (0.28)	0.956	c	
Classes <i>A</i> , <i>a</i> , and <i>U</i> .....	98	0.94 (0.13)	-0.38 (0.15)	0.734	c, d, e	
All cataloged clouds with estimated distances .....	131	{ 0.88 (0.13) 0.62 (0.074)	{ -0.28 (0.13) +0.020 (0.077)	{ 0.858 1.02	{ c, e c, f	
Classes <i>A</i> and <i>U</i> plus Dame <i>et al.</i> cloud complexes .....	61	{ 0.62 (0.044) 0.47 (0.045)	{ -0.077 (0.063) 0.12 (0.058)	{ 0.815 2.94	{ c g	1
Classes <i>A</i> , <i>a</i> , and <i>U</i> plus Dame <i>et al.</i> cloud complexes ...	130	0.62 (0.034)	-0.057 (0.047)	0.721	c, d, e	1
All cataloged clouds with estimated distances plus Dame <i>et al.</i> cloud complexes .....	163	{ 0.60 (0.034) 0.53 (0.031)	{ -0.021 (0.044) +0.086 (0.040)	{ 0.831 0.946	{ c, e c, f	1
Weighted mean parameter values .....		0.63 (0.05)	-0.071 (0.067)		h	
B. Data from Previous Publications						
LKM dark globules .....	16	0.48	-0.08		i, j	2
Myers and Benson NH <sub>3</sub> dense cloud cores .....	27	0.59 (0.2)	-0.023		i, j	3, 4
Sanders <i>et al.</i> giant molecular clouds .....	80	0.62 (0.05)	+0.16 (0.09)		j, k, l	5
Dame <i>et al.</i> cloud complexes .....	32	0.50 (0.05)	+0.11 (0.09)		j	1
Massachusetts-Stony Brook CO survey clouds .....	69	0.50 (0.05)	+0.26 (0.05)		j, k	6
Cepheus clumps .....	32	0.24 (0.06)	0.28		j	7
Ophiuchus clumps .....	89	0.28	+0.115		i, j	8, 9

<sup>a</sup> Tabulated parameters refer to least-squares fits assuming a power-law relation of millimeter spectral line width to cloud radius of the form in eq. (8) with radius in parsecs and line width expressed as equivalent width in km s<sup>-1</sup>.

<sup>b</sup> Formal errors, when available, are shown in parentheses.

<sup>c</sup> From a non-linear least-squares analysis with each datum weighted by the inverse of the corresponding variance. Distance errors assumed are 15% for clouds in Class *A*, 20% for those in class *U* and Dame *et al.* cloud complexes, and 50% for clouds in class *L* or *a*. Fractional errors assigned to cloud radii include estimates of the angular size uncertainties equal to  $7.5/a_{\text{maj}}$  in addition to a component due to distance uncertainty. The sum in quadrature of the formal errors in integrated CO emission and peak line intensity in the composite CO spectrum (eq. [5]) are used to derive errors in line width. Line widths quoted by Dame *et al.* (1986) are divided by 0.94 for consistency with the equivalent width velocity scale used here and are assigned 10% errors. The 17 local dark clouds with distance upper limits are not included in these fits.

<sup>d</sup> Eight class *a* clouds believed not to be associated with open clusters (see § V) are excluded.

<sup>e</sup> Class *a* clouds at cluster distances.

<sup>f</sup> Class *a* clouds at kinematic distances (see Table 8).

<sup>g</sup> Linear least-squares fit assuming zero error in cloud size.

<sup>h</sup> Excluding trials described by notes "f" or "g"; errors are derived as described in text.

<sup>i</sup> Includes correction for thermal line broadening, as originally reported.

<sup>j</sup> A constant was added to the published best-fit intercept for consistency with the equivalent width velocity scale.

<sup>k</sup> A constant was added to the published best-fit intercept to allow for fit to cloud radius instead of diameter (reported originally).

<sup>l</sup> Clouds apparently grouped by size into seven bins prior to least-squares fitting.

REFERENCES.—(1) Dame *et al.* 1986; (2) Leung, Kutner, and Mead 1982; (3) Myers and Benson 1983; (4) Myers 1983; (5) Sanders, Scoville, and Solomon 1985; (6) Solomon *et al.* 1987; (7) Carr 1988; (8) Loren 1988a; (9) Loren 1988b.

in the individual trials are consistent with these numbers given their associated formal errors. Thus, the best power-law relation between the cloud line widths and sizes in Figure 12b is of the form  $\Delta V \propto R^{0.6}$ . Note that a standard (linear) least-squares analysis which ignores the errors in cloud size systematically underestimates the slope,  $a_1$ , by about 24% (see Table 6A).

While some researchers have reported relations of line width to size for unrelated molecular clouds, others have measured an analogous relation for the distinguishable clumps in a single cloud. If structure in the interstellar medium is hierarchical and self-similar, the line width-size relation for clumps should resemble the line width-size relation for clouds. Previously published line width-size relations of both types are shown for comparison with our results in Table 6B and discussed separately below.

The clumps in a single molecular cloud all lie at nearly the same distance, so distance errors do not enter the calculation of the slope of the line width-size relation. Both Carr (1987) and Loren (1989a, b) studied the clumps in the nearby Cepheus and Ophiuchus clouds and found relatively flat relations of line width to clump size for clumps ranging in radius from a few

tenths to a few pc. Many of the clumps in both surveys are poorly resolved, however, and errors in clump size, like errors in distance, if neglected, lead to underestimation of the slope of the line width-size relation. This bias must affect the values for  $a_1$  shown in Table 6B for the Cepheus and Ophiuchus clumps, but it cannot be determined without reanalyzing the Carr (1987) and Loren (1989b) data whether the neglect of clump size errors implicit in the linear least-squares method can explain why the clumps appear to follow a flat line width-size relation relative to the larger molecular clouds. We also find what appears to be a modest flattening of the line width-size relation for clouds smaller than a few pc in radius. This can be seen on inspection of Figure 12a to be due in large part to the class *L* clouds; it is a matter to which we shall return in § Vc. Note that, on average, the line widths and sizes that characterize the clumps cataloged by Carr (1987) and Loren (1989a, b) are consistent with the line width-size relation derived from our fit to large clouds (see Fig. 12b). This general agreement would not be expected if the interclump gas in the Cepheus and Ophiuchus clouds exerts significant external pressure on the clumps in those clouds (Elmegreen 1989).

Most catalogs of molecular clouds include unrelated clouds at different distances. Dame *et al.* (1986) and Solomon *et al.* (1987) effectively ignored significant errors in cloud size by using the linear least-squares method to analyze their data; Leung, Kutner, and Mead (1982) apparently did so as well. Myers (1983) warned his readers that his least-squares fits were afflicted with the problem of underestimated relative errors in cloud size, but he felt that a more rigorous treatment was unwarranted given the scatter and limited dynamic range of the data he considered. In each of these cases, an unknown systematic underestimation of the line width–size relation slope is expected, and a slope less than 0.6 is reported. Sanders, Scoville, and Solomon (1985) first grouped their clouds in size bins then used the linear least-squares method to fit the mean line width at each bin. This method would have provided an unbiased estimate of the slope of the line width–size relation only if (a) the same number of clouds were in each bin, (b) the bin average cloud size had always been equal to the size at the bin center, and (c) the standard deviation of the sizes of clouds in each bin had always been sufficiently small. It is doubtful that all of these conditions were satisfied and impossible to predict without a detailed analysis how the unconventional fitting method influenced the derived slope, but the result was a line width–size relation slope in excellent agreement with ours. Had a rigorous, nonlinear regression analysis been applied to all the data used to measure the line width–size relation for molecular clouds, it is likely that a line of slope about 0.6 would have been found to describe adequately the observations over three orders of magnitude in cloud size from  $R \sim 0.1$ –100 pc.

#### b) The Mass-Radius and Density-Radius Relations

Even greater attention must be paid to the errors in a regression analysis of molecular cloud mass or density versus radius because cloud mass, as measured, is proportional to the cloud distance squared, while cloud radius is proportional to distance. This may give rise, depending on the relative magnitudes of the errors of measured quantities (CO line flux, cloud angular size, and distance) to an apparent relation of the form  $M \propto R^2$  which, in turn, could lead one to the erroneous conclusion that all molecular clouds have the same column density. In fact, a considerable investment has been made in trying to understand theoretically the significance of an  $M \propto R^2$  relation (e.g., Chièze 1987; Elmegreen 1989; Maloney 1988) or to attribute the  $R^2$  “law” to a conspiracy of observational selection effects (Kegel 1989), but, as shown below, the effort should be applied to an  $M \propto R^3$  relationship.

A proper analysis must allow for the fact that errors in mass due to uncertainty in cloud distance will be correlated with errors in cloud size due to the same uncertainty. This can be accomplished in one of two ways: (a) a least-squares fit to mass versus radius can be obtained in which off-diagonal elements of the covariance matrix of the data are allowed to be nonzero, or (b) a multivariate regression model can be employed in which the regressor variables are the measurable quantities CO line flux, cloud angular size, and distance. In (b), the errors may be assumed to be uncorrelated and the model parameters may be constrained such that, when an expression is derived from the fit for the relation of cloud mass to radius, there is no distance dependence. We consider method (b) to be somewhat less cumbersome than method (a), and we use the well-suited numerical least-squares method described by Jefferys (1980) to perform the analysis.

Consider a linear regression model of the form

$$\log S_{\text{CO}} = b_1 \log \theta + b_2 \log d + b_3, \quad (9)$$

in which  $S_{\text{CO}}$  is the CO line flux in  $\text{K km s}^{-1} \text{ deg}^2$ ,  $\theta$  is the cloud angular radius in degrees, and  $d$  is the distance in kpc. From equations (2) and (4), it can be seen that

$$M = k_M S_{\text{CO}} d^2, \quad (10a)$$

or

$$\log M = \log k_M + \log S_{\text{CO}} + 2 \log d, \quad (10b)$$

where  $k_M \simeq 1.3 \times 10^3 M_\odot \text{ K}^{-1} \text{ km}^{-1} \text{ s kpc}^{-2}$ , and  $M$  is measured in units of the solar mass. Also,

$$R = k_R \theta d, \quad (11a)$$

or

$$\log R = \log k_R + \log \theta + \log d, \quad (11b)$$

gives  $R$  in pc where  $k_R = 10^3 \pi / 180 \simeq 17.5 \text{ deg}^{-1}$ . Using equations (10b) and (11b) to eliminate  $\log S_{\text{CO}}$  and  $\log \theta$  in equation (9), one obtains

$$\log (M/k_M) = b_1 \log (R/k_R) + (2 - b_1 + b_2) \log d + b_3. \quad (12)$$

Thus, if one solves the least-squares problem subject to the parameter constraint

$$-b_1 + b_2 + 2 = 0, \quad (13)$$

then the resulting model will describe a relation between cloud mass and radius which is independent of distance, an arguably desirable condition. When the least-squares problem (9) is solved subject to the constraint equation (13), the inferred mass-radius relation (according to eqs. [12] and [13]) is

$$\log M = b_1 \log R + B, \quad (14)$$

where  $B = -b_1 \log k_R + b_3 + \log k_M$ .

Figure 13 is a log-log plot of the masses and radii of cataloged molecular clouds. Also shown in the figure is the best-fit

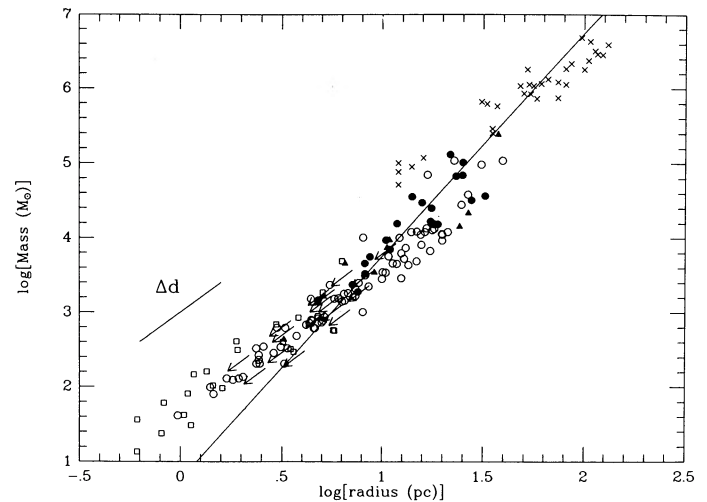


FIG. 13.—Masses and radii of cataloged molecular clouds. Symbols are the same as in Figure 12a. Crosses represent the large cloud complexes from the catalog of Dame *et al.* (1986). The line segment labeled  $\Delta d$  has slope 2 and shows the effect that distance errors have on the measurements. The line through the data is a least-squares fit (see text) to the class A, class U, and Dame *et al.* clouds only (see Table 7A).

TABLE 7  
EMPIRICAL MASS-RADIUS RELATIONS<sup>a</sup>

Cloud Sample	Number of Clouds	$b_1^b$	$B^b$	rms Residual	Notes	References
A. This Paper						
Classes <i>A</i> and <i>U</i> .....	29	3.40 (0.44)	0.25 (0.52)	0.911	c	
Classes <i>A</i> , <i>a</i> , and <i>U</i> .....	98	3.08 (0.15)	0.64 (0.17)	0.631	c, d, e	
All cataloged clouds with estimated distances .....	131	{ 2.89 (0.12) 2.52 (0.069)	{ 0.89 (0.13) 1.32 (0.072)	{ 0.741 0.842	{ c, e c, f	
Classes <i>A</i> and <i>U</i> plus Dame <i>et al.</i> cloud complexes .....	61	2.99 (0.15)	0.76 (0.21)	0.911	c	
Classes <i>A</i> , <i>a</i> , and <i>U</i> plus Dame <i>et al.</i> cloud complexes ...	130	2.99 (0.088)	0.76 (0.11)	0.707	c, d, e	1
All cataloged clouds with estimated distances plus Dame <i>et al.</i> cloud complexes .....	163	{ 2.89 (0.078) 2.68 (0.063)	{ 0.91 (0.096) 1.19 (0.076)	{ 0.771 0.861	{ c, e c, f	1
Weighted mean parameter values .....		2.95 (0.11)	0.82 (0.14)		g	
B. Data from Previous Publications						
LKM dark globules .....	16	2.29	2.25		h	2
Myers and Benson NH <sub>3</sub> dense cloud cores .....	27	2.0 (0.2)	2.58		i	3, 4
Perseus arm and Orion Clouds .....	94	2.77 (0.11)	1.16			5
Sanders <i>et al.</i> giant molecular clouds .....	80	2.24 (0.10)	2.66 (0.19)		j	6
Dame <i>et al.</i> cloud complexes .....	32	1.7 (0.1)	3.01 (0.18)		i	1
Massachusetts-Stony Brook CO survey clouds .....	69	2.47 (0.22)	2.06 (0.20)		k	7
Cepheus clumps .....	32	2.51 (0.06)	1.81		h	8
Ophiuchus clumps .....	89	3.02	3.07			9, 10

<sup>a</sup> Tabulated parameters refer to least-squares fits assuming a power-law relation of cloud mass to radius of the form in eq. (14) with mass in solar units and radius in parsecs.

<sup>b</sup> Formal errors, when available, are shown in parentheses.

<sup>c</sup> From the constrained regression analysis described in § IVb. Each datum is weighted by the inverse of the corresponding variance. Distance errors assumed are 15% for clouds in class *A*, 20% for those in class *U* and Dame *et al.* cloud complexes, and 50% for clouds in class *L* or *a*. Cloud angular sizes are assigned fractional errors equal to the survey sampling interval, 7.5, divided by the major axis length,  $a_{\text{maj}}$ . Errors in  $S_{\text{CO}}$  are formal errors derived from the number of lines of sight containing emission from the cloud, the number of spectrometer channels over which the cloud emission is summed, and the rms baseline noise. The 17 local dark clouds with distance upper limits are not included in these fits.

<sup>d</sup> Eight class *a* clouds believed not to be associated with open clusters (see § V) are excluded.

<sup>e</sup> Class *a* clouds at cluster distances.

<sup>f</sup> Class *a* clouds at kinematic distances (see Table 8).

<sup>g</sup> Excluding trials described by note “f”; errors are derived as described in text.

<sup>h</sup> A constant was added to the quoted intercept to allow for the helium contribution to cloud mass (not originally included).

<sup>i</sup> Derived from published relation of particle density to radius assuming uniform spherical cloud.

<sup>j</sup> Derived from line width–size relation using the published density model which assumes clouds are in virial equilibrium.

<sup>k</sup> Derived from published empirical relations and assumption that cloud mass is proportional to CO line luminosity as in eq. (4) of this paper.

REFERENCES.—(1) Dame *et al.* 1986; (2) Leung, Kutner, and Mead 1982; (3) Myers and Benson 1983; (4) Myers 1983; (5) Casoli, Combes, and Gerin (1984); (6) Sanders, Scoville, and Solomon 1985; (7) Solomon *et al.* 1987; (8) Carr 1987; (9) Loren 1988a; (10) Loren 1988b.

line from the regression analysis described above. Least-squares fits were obtained for a variety of cloud samples. Results of these trials are summarized in Table 7A. As expected, underestimation of the error in cloud distance biases the fit value of  $b_1$  toward 2. Consistent values for the fit parameters are obtained with the different assumptions if realistic errors are assigned (see footnote *c* in Table 7). The data are reasonably well described by the following power-law relation between cloud mass and radius:

$$\log M \simeq (2.95 \pm 0.11) \log R + (0.82 \pm 0.14). \quad (15)$$

Note that the power-law index, or slope (parameter  $b_1$ ), is about 3 and the “intercept” or, equivalently, the mass of a cloud of radius 1 pc (derived from eq. [14], and the fit parameters) is about  $4\text{--}8 M_{\odot}$ . The parameters in equation (15) are averages of the parameters from the trials in Table 7A weighted by their respective formal errors. The errors assigned to the parameters in equation (15) reflect the variation from trial to trial, not just the formal errors. Given their associated formal errors, the parameters in the individual trials are consistent with the numbers in equation (15).

Corresponding to the derived relation between mass and cloud size is a relation between mean density and size. The

mean H<sub>2</sub> molecule number density is given by the relation

$$\log \langle n(\text{H}_2) \rangle = \log k_n + \log M - 3 \log R, \quad (16a)$$

or, upon using equation (14) for  $\log M$ ,

$$\log \langle n(\text{H}_2) \rangle = (b_1 - 3) \log R + \log k_n + B, \quad (16b)$$

where  $k_n = 3M_{\odot}/(4\pi\mu p^3)$ ,  $M_{\odot} = 1.99 \times 10^{33} \text{ g } M_{\odot}^{-1}$ ,  $p = 3.09 \times 10^{18} \text{ cm } \mu\text{pc}^{-3}$ , and  $\mu$  is the mean molecular weight per H<sub>2</sub> molecule, 2.72 amu. Thus,  $k_n \simeq 3.58 \text{ cm}^{-3} M_{\odot}^{-1} \mu\text{pc}^3$ , so the density analog of equation (15) is

$$\log \langle n(\text{H}_2) \rangle \simeq (-0.05 \pm 0.11) \log R + (1.37 \pm 0.14). \quad (17)$$

Note that exactly the same least-squares problem (eq. [9]) subject to the same parameter constraint (eq. [13]) would have to have been solved to calculate the relation between  $\langle n \rangle$  and  $R$  directly, so it is of no consequence that the density-radius relation in equation (17) was derived from the empirical mass-radius relation (eq. [15]) rather than from an “independent” least-squares solution. Equation (17) implies that *the mean H<sub>2</sub> molecule density is nearly constant from cloud to cloud, about 20 H<sub>2</sub> cm<sup>-3</sup>, independent of cloud size.* Much of the spread in the density distribution shown in Figure 4, therefore, must be attributed to measurement errors.

The above result implies that the average  $H_2$  column density increases linearly with increasing cloud size; it is not constant, as would be implied by  $M \propto R^2$ . Whereas one might suspect selection effects as the source of a relation of the form  $M \propto R^2$  (Kegel 1989), it is less likely that selection effects could conspire to make interstellar clouds appear to have constant volume density. Thus, our result lends itself to arguments that the CO  $J = 1 \rightarrow 0$  line “sees through” molecular clouds even if the regions that are responsible for the line emission are optically thick at the rest frequency of the line, as is widely believed to be true.

Some mass-radius relations reported elsewhere are given in Table 7B for comparison with the relation derived here (see Table 7A or eq. [15]). Previously published values for the slope of this relation are in the range 1.7–3, but none of the least-squares fits from which these values were derived allowed for the possibly correlated errors in mass and radius (see above). Note that if, for some reason, the random errors in cloud distance were sufficiently small in some sample of clouds relative to the other measurement errors, then errors in cloud mass and size would be effectively uncorrelated, and the bias in the slope of the mass-radius relation toward a value of 2 would become insignificant. This may have been the case for the clouds studied by Casoli, Combes, and Gerin (1984), because the clouds they studied were concentrated in the Perseus and Orion Galactic spiral features, and also for the clouds studied by Carr (1987) and Loren (1989*a, b*), because their “clouds” were inside larger clouds and thus were all at about the same distance. As expected, Casoli, Combes, and Gerin (1984), Carr (1987), and Loren (1989*a*) derived mass-radius relation slopes consistently larger than those derived from cloud samples plagued by the problem of correlated errors (see Table 7B). Using the method described above, we fit our data in a manner that allowed for the error correlations and derived a mass-radius relation in reasonable agreement with the relations derived by Cassoli, Combes, and Gerin, Carr, and Loren. Thus we may conclude with some confidence that the masses of molecular clouds are related to their sizes by a power law of slope approximately 3.

### c) Are Molecular Clouds in Virial Equilibrium?

Virial equilibrium is a condition in which the moment of inertia of a system changes either at a constant rate or not at all. This condition can occur only when the net force acting on the system, or on each similar element of the system, is zero. No net mass exchange occurs, for example, among the parts of a system in virial equilibrium.

In general, a cloud can be said to be in virial equilibrium when the internal magnetic (see, e.g., Myers and Goodman 1988), thermal, and turbulent pressures (see, e.g., Larson 1981; Scalo 1987), plus the systemic rotation (see, e.g., Kleiner and Dickman 1985), prevent collapse by balancing the external pressure (see, e.g., Chièze 1987; Maloney 1988) and the cloud’s gravity; however, not all these factors are important in every case. For example, the thermal pressure,  $P_{th}$ , is negligible when  $P_{th} R^4 / (GM^2) \ll 1$ , a condition that obtains when  $R$  (pc)  $\gg 10^{-4} (T_k/10 \text{ K})^{1/2} \langle n \rangle / 20 \text{ H}_2 \text{ cm}^{-3})^{-1/2}$  for cloud radius  $R$ , kinetic temperature  $T_k$ , and mean density  $\langle n \rangle$ . Similarly, a cloud of mass  $M$  and average mass density  $\rho$  cannot be supported by magnetic pressure if  $3GM/(5R) \gg B^2/(8\pi\rho)$ , where  $B$  is the magnetic field strength. The molecular cloud magnetic field data tabulated by Myers and Goodman (1988) can be described approximately by the empirical relation  $B \approx 10 \mu\text{G}$

(pc) $^{-1}$  for  $10^{-2} < R$  (pc)  $< 26$ . Thus, the magnetic pressure is unimportant when  $R$  (pc)  $\gg 4 (\langle n \rangle / 20 \text{ H}_2 \text{ cm}^{-3})^{-1/2}$ . Rotation can be ignored if  $I\omega^2 \ll 3GM^2/(5R)$ , where  $I$  is the moment of inertia of the cloud and  $\omega$  is its angular rotation speed. This condition is equivalent to  $\omega \ll (2\pi G\rho)^{1/2}$ , or  $\omega \ll 0.19 \text{ km s}^{-1} \text{ pc}^{-1} (\langle n \rangle / 20 \text{ H}_2 \text{ cm}^{-3})^{1/2}$ .

Because most of the clouds found in the open cluster CO survey are larger than a few parsecs in radius and do not have large radial velocity gradients across their projected surfaces, thermal, magnetic, and rotational terms in the equation for virial equilibrium are not included in the following discussion. Furthermore, the cataloged clouds do not obey a mass-radius relation of the  $M \propto R^2$  form predicted by models in which molecular clouds are in pressure equilibrium with the ambient interstellar medium (Chièze 1987; Maloney 1988). Thus, we consider a narrow definition of virial equilibrium, namely the balance of a cloud’s gravitational potential energy by the kinetic energy,  $T$ , of macroscopic motion in its interior. We refer to this motion as “turbulence,” but the following argument is valid even if there is a systematic component to the motion, provided that the observed hyperthermal CO line widths of molecular clouds measure  $(2T/M)^{1/2}$ .

To be in virial equilibrium in the narrow sense, a cloud must satisfy the condition  $2T + \Omega = 0$ , where  $T = (\frac{1}{2})MV_{\text{turb}}^2$  and  $\Omega = -\Gamma GM^2/R$  for cloud mass  $M$ , radius  $R$ , and internal “turbulent” velocity  $V_{\text{turb}}$ . The factor  $\Gamma$  depends on the cloud geometry and mass distribution, is  $\frac{3}{2}$  for a uniform, spherical cloud, and in general is less than or about 1. Therefore, the turbulent velocity for a cloud in virial equilibrium is equal to the “virial velocity” given by

$$V_{\text{vir}} \equiv (\Gamma GM/R)^{1/2}. \quad (18)$$

According to equation (18), molecular clouds that obey a mass-radius relation such that  $M \propto R^\alpha$  must obey a relation between  $V_{\text{turb}}$  and radius such that  $V_{\text{turb}} \propto R^\beta$ , where  $\beta = (\alpha - 1)/2$  if they are in virial equilibrium. In practice,  $V_{\text{turb}}$  is derived from the CO data with the assumption that gas motions within clouds are random and isotropic, since only the one-dimensional velocity dispersion can be measured (see, e.g., Leung, Kutner, and Mead 1982; Myers 1983; Loren 1989*a*); under this premise,  $[3/(2\pi)]^{1/2} \Delta V_{\text{eqw}}$  is used to give the turbulent velocity, where  $\Delta V_{\text{eqw}}$  is the equivalent width of the composite CO spectral line (eq. [7]). Thermal broadening of the observed spectral lines is negligible. In § IVb, it was shown that  $\alpha \approx 2.95$ . Thus if clouds are in virial equilibrium, we expect to find a relation between CO line width and size such that  $\Delta V_{\text{eqw}} \propto R^{0.97}$ . Except for a few restricted samples of clouds (see Table 6), this relation differs significantly from the observed power-law relation between  $\Delta V_{\text{eqw}}$  and  $R$ , which has an index of about 0.6 (eq. [8]).

This difference can be seen in Figure 14. The figure shows, as a function of cloud radius, the ratio  $[3/(2\pi)]^{1/2} \Delta V_{\text{eqw}} / V_{\text{vir}}$ , where  $V_{\text{vir}}$  is derived from the cloud mass and radius using equation (18). The line width ratio is a decreasing function of  $R$  and is greater than one in all but a few cases. In Figure 15 we show the distribution of line width ratios for the cataloged clouds whose distances are the most reliably determined, namely those known to be associated with photometrically studied open clusters (i.e., class A clouds). The mean line width ratio for these relatively large clouds is  $1.95 \pm 0.15$  (standard deviation of the mean; hereafter abbreviated as “s.d.o.m.”), a value that may be of interest because it is close to the value (1.83) expected if internal motions in the clouds are as fast as

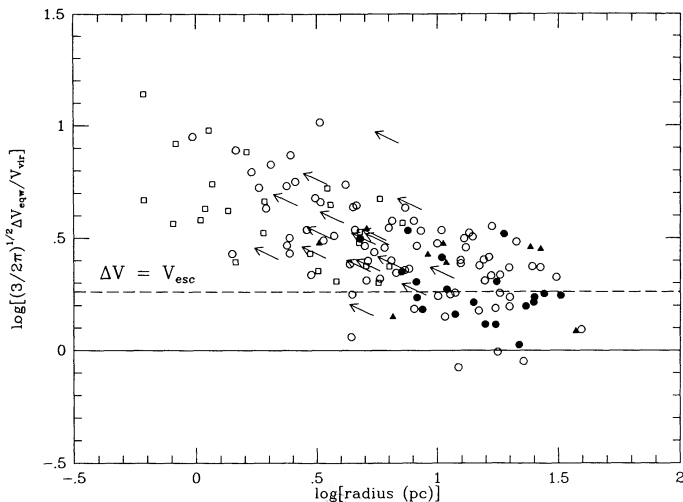


FIG. 14.—The ratio of observed to virial line width, a measure of the deviation from virial equilibrium, is shown as a function of cloud radius. Symbols are the same as in Figure 12a. For clouds in virial equilibrium,  $(3/2\pi)^{1/2}\Delta V_{eqw}$  should equal  $\Delta V_{vir}$  (solid line). Large clouds have line-widths approximately equal to the value expected if motions in their interiors are as great as the escape velocity (dashed line; also see Fig. 15).

the escape velocity,  $(2GM/R)^{1/2}$ . Note that underestimation of the constant that relates the  $H_2$  column density to the CO line intensity in equation (3), or any other failure to account for the entire mass of a cloud, would lead to an apparent line width ratio greater than one, but it could not easily explain the fact that small clouds are further from equilibrium than larger ones; an additional hypothesis that small clouds contain more of the “missing mass” (e.g., a greater number of disassociated molecules) than larger clouds would be required to account for the observations. Although the observed behavior, which corresponds to a power-law index,  $\beta$ , flatter than  $(\alpha - 1)/2$ , is expected if magnetic fields or thermal pressure lend significant support to molecular clouds, turbulent pressure arguably provides the support for the clouds described here (see above), so one would be well advised to consider the simple possibility

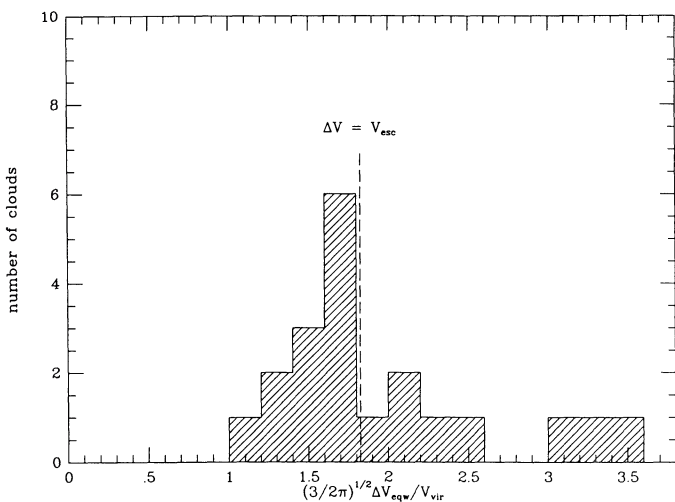


FIG. 15.—Distribution of the ratio of observed to virial line width for clouds in class A. The ratio typically is greater than 1. Note that the observed line widths cluster around the cloud escape velocity (vertical dashed line).

that the clouds are not, in general, in virial equilibrium (Maloney 1990).

#### d) Relaxation Conditions for a Clumpy Cloud

Is it reasonable to suppose that molecular clouds are not in virial equilibrium, and what can be inferred about their nature in this case? These questions can be addressed by looking at the time scales on which various physical phenomena act to affect the behavior of clouds for, if it should turn out that clouds are perturbed frequently or have short lifetimes, they may not have time to relax to a state of equilibrium.

Evidently, to be successful, a molecular cloud theory must allow for the fact that the clouds appear to be internally clumpy. The relevant physical processes (except those involving interactions of a cloud with the ambient interstellar medium), and the time scales on which they operate, were considered by Pumphrey and Scalo (1983, hereafter PS); the following discussion parallels theirs.

Let us suppose that molecular clouds form at sites of small density fluctuations in an otherwise approximately homogeneous interstellar medium and that density enhancement occurs initially as a result of “free-fall” collapse when self-gravity overcomes thermal pressure. The time required for free-fall collapse to progress to a singularity,  $\tau_{ff}$ , is a function of the initial density,  $n_0$ :

$$\tau_{ff} \approx \left( \frac{3\pi}{32G\mu n_0} \right)^{1/2} \approx 31n_0^{-1/2} \text{ Myr}. \quad (19)$$

But suppose the cloud fragments into “clumps” long before it collapses completely (see, e.g., Woolfson 1978). If the clumps were to accelerate under the influence of their collective gravitational potential, they would at some point reach a velocity equal to the virial velocity prescribed by equation (18). It can be shown that this will occur when the cloud radius is 70% of its initial radius and, if its mass is conserved in this time, its density will have increased by a constant factor 2.9. The constant observed cloud density (eq. [17]) would then be consistent with collapse from a uniform diffuse interstellar medium if any subsequent changes in the mean cloud density were small. The time required for this violent relaxation,  $\tau_{vr}$ , can be shown to be approximately  $(2.08/\pi)\tau_{ff}$ . If the clump motions were randomized in the violent relaxation of the cloud, then  $\tau_{vr}$  would be the time required to *establish* virial equilibrium. Since molecular clouds may have lifetimes significantly greater than  $\tau_{vr}$ , the key issue, which we now proceed to address, is: What conditions must be satisfied for virial equilibrium to be *sustained*?

Clumps in a cloud may collide with other clumps, experience drag due to their passage through the interclump gas, and respond to the overall gravitational field of the cloud. PS found that tidal encounters of clumps with each other typically result in very little internal heating or mass loss and can be neglected. They also showed that direct collisions among clumps more effectively decelerate them than drag due to the interclump gas unless the clumps contain less than 20% of the cloud mass. For the sake of argument, we ignore the interclump gas.

The importance of direct clump-clump collisions for the evolution of cloud structure is evident in the fact that the geometrical collision time scale,  $\tau_{cc}$ , is typically only a fraction of the crossing time,  $\tau_{cross}$ , or the free-fall time. In particular, if  $\tau_{cross}$  is defined as  $2R/V_{turb}$ , then

$$\tau_{cc}/\tau_{cross} = 24^{-1/2}f_A^{-1}, \quad (20)$$

where  $f_A$  is the relative clump projected area,  $N_c(r_c/R)^2$  for  $N_c$  clumps of average radius  $r_c$ . Gravitational focusing, which would shorten the clump-clump collision time slightly, was shown by PS to be unimportant in cases of interest. For a cloud to be recognized as such,  $f_A$  must be greater than or about equal to 1, so  $\tau_{cc} < \tau_{cross}$ . For a uniform, spherical cloud in virial equilibrium,  $\tau_{cross} \simeq 2.33\tau_{ff}$  (if  $\tau_{ff}$  is evaluated at the cloud's mean density) in which case  $\tau_{cc}/\tau_{ff} \simeq 0.48/f_A$ . Despite their greater density, the clumps themselves are not expected to collapse in a time shorter than the free-fall collapse time for the cloud if they are internally turbulent (Bonazzola *et al.* 1987).

To understand the dynamical evolution of a cloud, one must, in principle, understand how the clumps behave when they collide. Fragmentation, coalescence, and shock dissipation of relative kinetic energy are all likely to be important processes, and ablation and drag may play a role depending on how much interclump gas is present. In any case, as PS were careful to point out, the appropriate cross section for a particular interaction may differ significantly from the geometric cross section ( $4\pi r_c^2$  if all the clumps are the same size). For example, Scalo and Pumphrey (1982) introduced the dimensionless parameter  $\chi$  relating the cross section for the dissipation of a cloud's turbulent energy to the geometric cross section by  $\sigma_{dis} = \sigma_{geom}/\chi$ , and they found by executing a series of numerical simulations in which the effect of gravity was included that  $\chi$  is approximately 10 (Scalo and Pumphrey 1982; J. M. Scalo 1989, private communication);  $\chi$  is greater than 1 because not all the relative kinetic energy is dissipated in each collision of two clumps. Hence, the turbulent dissipation time,  $\tau_{dis}$  ( $\sim \chi\tau_{cc}$ ), is longer than the clump-clump collision time by a factor of about 10.

Following Scalo and Pumphrey (1982), we introduce a dimensionless parameter  $\Omega$  to describe the randomization of the clump velocity vectors and the corresponding relaxation of the velocity distribution. Clump trajectories are reoriented both by physical collisions and long-range scattering in the gravitational field of the cloud, and the mechanism that most rapidly produces a cumulative deflection in the clump trajectory by some angle, say  $90^\circ$ , determines the relaxation time. Let  $\Omega^{-1}$  be the effective cross section for  $90^\circ$  deflection by physical collisions in units of the geometric cross section; in other words,  $\sigma_{90} = \sigma_{geom}/\Omega$ . Then  $\Omega\tau_{cc}$  is the time required for collisions of clumps to result in relaxation of the clump velocity distribution.

Now let the dynamical relaxation time,  $\tau_{dr}$ , be the time required for a clump, in response to long-range gravitational scattering, to undergo a net  $90^\circ$  deflection;  $\tau_{dr}$  is essentially the energy exchange time (Chandrasekhar 1942), or the similar relaxation time (Spitzer and Härm 1958) for a star cluster. Since the relaxation time is always much greater than the crossing time which, in turn, is greater than the clump-clump collision time,  $\tau_{dr} \gg \tau_{cc}$ . The time scale ratio  $\tau_{dr}/\tau_{cc}$  (see, e.g., PS, their eq. [16]), gives the number,  $N_{pc}$ , of direct physical collisions of clumps that occur in the time  $\tau_{dr}$ . For example,  $N_{pc}$  is approximately 75 for a cloud in which 1000 independent clumps fill 1% of the cloud volume. Although in general  $N_{pc} \gg 1$ , not every clump-clump encounter results in a  $90^\circ$  trajectory reorientation, as might nearly be the case if the clumps were hard elastic spheres.

In the case  $\Omega\tau_{cc} > \tau_{dr}$  (i.e.,  $\Omega > N_{pc}$ ), the clump motion is dominated by long-range gravitational scattering, and relaxation of the velocity distribution to an equilibrium, approximately Maxwellian (Spitzer and Härm 1958), state would

occur in a time about equal to  $\tau_{dr}$ . This condition would apply if the clumps themselves were essentially ensembles of point masses. Considering the apparently hierarchical nature of the interstellar medium (Scalo 1985), such an idealization might be suitable depending on the smallest characteristic scale size of the structure.

On the other hand, if the clumps are relatively homogeneous and experience shocks when they collide, or if they are suffused with enough ionized gas and tied together by magnetic fields (Clifford and Elmegreen 1983; Falgarone and Puget 1986), their motions can be expected to be more drastically altered when they collide, and  $\Omega$  may be less than  $N_{pc}$ . If  $N_{pc} > \Omega$ , more than enough physical collisions occur in a time  $\tau_{dr}$  to deflect the clumps by  $90^\circ$ , and relaxation of the clump velocity distribution, presumably not to a Maxwellian distribution (see, e.g., PS, their Fig. 11), should occur in a time about equal to  $\Omega\tau_{cc}$ .

In any case, the clump velocity distribution should relax on a time scale,  $\tau_{rel}$ , bounded on the low side by  $\tau_{cc}$ , and on the high side by  $\tau_{dr}$ , and we can write  $\tau_{rel} = \Omega\tau_{cc}$ , where  $1 < \Omega < N_{pc}$ . In a sense,  $\Omega$  is a measure of how well clumps "remember" their trajectories; a bigger value of  $\Omega$  means more collisions are required for a clump to forget its collision history. Detailed, realistic numerical simulations of clump-clump collisions, such as those of Stone (1970), Hausman (1981), and Gilden (1984) can, in principle, be used to estimate  $\Omega$ . Two 1000-body simulations with "memoryless" collisions (PS) suggest that the velocity distribution relaxes in a time about equal to  $30\tau_{cc}$ . To allow for the fact that real collisions may not be perfectly memoryless, one might assume that  $\Omega$  is greater than 30, but it is not clear that this assumption would apply to a cloud with an initial number of clumps fewer than 1000.

If the velocity distribution has a characteristic dispersion close to the equilibrium value long before strict virial equilibrium is established, then the greater than virial observed CO line widths may not be explained simply by concluding that the clouds are not in virial equilibrium. Indeed, the foregoing premise may be true for a self-gravitating, collisionless system, or a system in which the collisions are elastic, but neither of these conditions are applicable to the collisions of clumps in a molecular cloud. Some loss of relative kinetic energy undoubtedly occurs as the clumps in a cloud collide. As a result, in the absence of a source of mechanical energy, the systemic velocity dispersion must decrease monotonically. The numerical simulations of PS (see their Fig. 11) follow this trend and show, furthermore, that the velocity distribution in a system in which the collisions are inelastic is not Maxwellian.

Returning to the central issue, for virial equilibrium to be sustained, the relaxation time must be much shorter than the cloud lifetime (Kutner 1984). Considerable effort has been invested in assessing the lifetimes of molecular clouds. The fact that massive clouds ( $> 10^6 M_\odot$ ) appear to be confined to galactic spiral arms (see, e.g., Bash and Peters 1976; Dame *et al.* 1986; Vogel, Kulkarni, and Scoville 1988) is an indication that those clouds have lifetimes that do not exceed a few times  $10^7$  yr. No similar observational constraint exists for small clouds; the lifetimes of such clouds could exceed a spiral arm crossing time,  $\sim 10^8$  yr. If the cloud lifetime is equal to the theoretical turbulent dissipation time, then the condition  $\Omega \ll \chi$  must be satisfied for clouds to remain in equilibrium. Numerical simulations (PS; Scalo and Pumphrey 1982) imply that  $\Omega$  is greater than  $\chi$ , however, and therefore they lead to the

conclusion that equilibrium cannot be maintained. Further support for this conclusion can be found in the two-dimensional cloud collision simulation of Stone (1970). Unfortunately, the premise that the cloud lifetime is approximately equal to the turbulent dissipation time leaves the above argument vulnerable, since neither of these time-scales is well known.

Another condition for equilibrium to be maintained is that  $\tau_{\text{rel}}$  must be short compared to the time for the cloud to suffer a significant perturbation. For example, Stone (1970) concluded from a hydrodynamical simulation of colliding clouds that a state of hydrostatic equilibrium cannot be restored in the time between successive collisions. One kind of perturbation is that experienced as a cloud is impacted by other interstellar clouds (see, e.g., Bash, Hausman, and Papaloizou 1981). A measure of how long it takes for such encounters to affect a cloud significantly is the time required for a cloud to sweep up its own mass of interstellar gas,  $\tau_{\text{sw}}$ . Let  $n$  be the  $\text{H}_2$  molecule density in the target cloud and let  $n_{\text{ISM}}$  be the mean H atom density in the interstellar medium. Then  $\tau_{\text{sw}} \simeq (8R/3V)(n/n_{\text{ISM}})$ , where  $R$  is the target cloud radius and  $V$  is its velocity relative to the ambient medium which we take to be the rms velocity of molecular clouds measured by Stark (1979),  $\sim 8 \text{ km s}^{-1}$ . In terms of the clump-clump collision time,

$$\tau_{\text{sw}} \simeq \left( \frac{8\sqrt{6}}{3} \right) f_A \left( \frac{V_{\text{turb}}}{V} \right) \left( \frac{n}{n_{\text{ISM}}} \right) \tau_{\text{cc}}. \quad (21)$$

If  $n/n_{\text{ISM}} \sim 20$ , equation (21) implies that  $\tau_{\text{sw}}/\tau_{\text{cc}} \simeq 16f_A(V_{\text{turb}}/1 \text{ km s}^{-1})$ , from which it follows that  $\tau_{\text{sw}}/\tau_{\text{rel}} \simeq 0.5f_A(V_{\text{turb}}/1 \text{ km s}^{-1})(\Omega/30)^{-1}$ . Whether the condition,  $\tau_{\text{sw}}/\tau_{\text{rel}} \gg 1$ , for clouds to stay in virial equilibrium is satisfied depends on how much greater than  $1f_A$  is, and on the poorly determined value of  $\Omega$ . If  $f_A$ , the relative clump projected area, is not much greater than 1, it would not be surprising to find molecular clouds out of equilibrium.

Other perturbing forces thought to affect molecular clouds on comparably short time scales are present as well (Kutner 1984). Some examples are winds from embedded low-mass stars (Norman and Silk 1980), shock waves from expanding H II regions, and supernovae which may transfer energy to clouds as Alfvén waves propagating along magnetic field lines, or as sound waves (Ferrière, Zweibel, and Shull 1988).

We are thus led to speculate on a possible explanation for the observations, illustrated in Figures 14 and 15, that clouds of all sizes found in the open cluster CO survey have line widths wider than the equivalent virial line width given by equation (18), and that small clouds appear to be further from virial equilibrium than bigger ones. Suppose that the clumps in all clouds are essentially the same. Then the product of  $f_A$  and  $V_{\text{turb}}$ , and hence the ratio  $\tau_{\text{sw}}/\tau_{\text{rel}}$ , increases with cloud size roughly as  $R^{1.6}$ , which implies that small clouds have a harder time staying in equilibrium than larger ones. Of course, any perturbation that affects small clouds more severely than bigger ones; not just collisions with other interstellar clouds, could produce the observed divergence of clouds from equilibrium with decreasing cloud size. Furthermore, the relaxed clump velocity distribution predicted in the numerical experiments of PS contains a disproportionate number of fast-moving clumps relative to a Maxwellian distribution with the same mean clump speed and may explain the greater than virial line widths; the non-Maxwellian form of the distribution is a consequence of the dissipative and disruptive nature of clump-clump collisions. In this interpretation,  $\Omega$  must be greater than or about equal to  $30f_A$  for clouds of all sizes.

Traditionally, molecular clouds have been thought of as isolated, relaxed systems in which self-gravity is balanced by turbulent pressure, and perhaps other kinds of pressure, but a fundamentally different interpretation is possible. Considering that the clouds exchange mechanical as well as radiative energy with their environments, they are not strictly closed systems, and they may not remain in virial equilibrium.

There are a few potential problems with the proposed hypothetical interpretation of molecular cloud observations. An obvious weakness is in the implied premise that clumps of molecular gas survive as independent entities as they undergo collisions; a good theory for the response of compressible turbulence to driving and damping forces is needed. Coalescence of the clumps might be expected to reduce the relative clump projected area,  $f_A$ , thereby increasing the susceptibility of clouds to perturbations. A less serious problem is that, contrary to our supposition, the clumps in all clouds, or even the clumps in a single cloud, are not likely to be the same. If the abolition of this condition means that  $\tau_{\text{sw}}/\tau_{\text{rel}}$  is not an increasing function of cloud size, then small clouds would not be expected to be more vulnerable than larger ones to perturbations of the kind considered. Finally, it is not clear how one might reconcile the supposition that clouds are composed of denser clumps with the fact that all the cataloged clouds have approximately the same mean density. One would either have to believe that the clumps are denser *because* they are parts of clouds, or be able to find independently existing dense clumps in the interstellar medium out of which the larger clouds could form. It might be argued that the small dark clouds cataloged by Barnard (1927) or Lynds (1962), or the local dark clouds cataloged here (see § Vc), resemble the clumps in larger clouds.

## V. CHARACTERISTICS OF THE MOLECULAR CLOUDS ASSOCIATED WITH OPEN CLUSTERS

### a) Are Class a Clouds Associated with Clusters?

Class *a* clouds are distinct from local dark clouds in radial velocity and in their apparent obscuration of background stars; and whereas clouds assigned to class *A* exhibit compelling evidence of association with the clusters near which they are found, such evidence does not exist for the clouds assigned to class *a* (see § III). Since about half the cataloged clouds are of class *a*, it is desirable to make some assessment of the likelihood that these clouds actually are associated with the clusters.

There is no direct evidence of interaction of the clusters with class *a* clouds, but information about the cloud distances can be used to evaluate the possibility that they are located near the clusters. Two independent methods are used to estimate the distances of class *a* clouds: (1) a kinematic distance is derived based on the cloud radial velocity and a model for the Galactic rotation curve (Brand 1986), and (2) the empirical line width–size relation derived in § IVa is used with a cloud's CO line width to gauge its linear size, and a distance is inferred from its angular extent. Although both methods yield large distance uncertainties, one can still conclude that some class *a* clouds are unlikely to be associated with the clusters near which they are found because the cloud and cluster distances differ significantly.

Two distance estimates, based on the methods just described, are given for each class *a* cloud in Table 8. Also tabulated is the distance of the cluster near which the cloud was found and the number of standard deviations by which the

TABLE 8  
ESTIMATED DISTANCES OF CLASS *a* CLOUDS

Cloud	I/C	$d_{cl}^a$ (kpc)	$d_{ls}^b$ (kpc)	$\sigma_{d_{ls}}^c$ (kpc)	$\Delta^d$	$d_{kin}^e$ (kpc)	$d_{kin}$ Range <sup>f</sup> (kpc)	Cloud	I/C	$d_{cl}^a$ (kpc)	$d_{ls}^b$ (kpc)	$\sigma_{d_{ls}}^c$ (kpc)	$\Delta^d$	$d_{kin}^e$ (kpc)	$d_{kin}$ Range <sup>f</sup> (kpc)
NGC 6709C	I	0.93	1.46	(0.55)	1.0	0.4	0.0–1.1	NGC 433D <sup>i</sup>	I	4.50	1.73	(0.34)	8.1	0.9	0.1–1.7
NGC 6823B <sup>g,h</sup>	C	2.70	1.77	(0.16)	5.7	4.4	2.3–6.4	NGC 663A	I	2.53	2.54	(0.25)	0.0	3.1	2.2–4.2
NGC 6823C <sup>g,h</sup>	I	2.70	19.81	(3.23)	5.3	4.4	2.6–6.2	NGC 663B	I	2.13	2.23	(0.38)	0.3	3.0	2.0–4.0
NGC 6823D <sup>g</sup>	I	2.70	3.01	(0.50)	0.6	4.2	2.0–6.4	NGC 663C <sup>i</sup>	I	2.53	1.04	(0.07)	21.9	1.1	0.3–2.0
NGC 6823E	C	2.70	5.69	(1.17)	2.6	2.6	1.4–7.2	Stock 5A	C	1.60	1.54	(0.27)	0.2	0.5	0.0–1.3
Roslung 4B	I	2.90	3.93	(0.30)	3.5	1.7	0.4–6.4	Stock 5B	C	1.60	2.64	(0.78)	1.3	0.7	0.0–1.5
NGC 7067E	I	3.50	3.64	(1.80)	0.1	3.8	2.6–4.9	Stock 5C <sup>i</sup>	I	1.60	0.85	(0.13)	6.0	0.6	0.0–1.4
IC 1396C	I	0.80	1.91	(0.25)	4.4	0.2	0.0–1.8	Stock 5D <sup>h</sup>	I	1.60	1.81	(0.15)	1.4	0.1	0.0–0.9
IC 1396D	I	0.80	0.99	(0.12)	1.6	0.2	0.0–1.7	Stock 5E	C	1.60	1.14	(0.44)	1.1	0.4	0.0–1.2
NGC 7160A	C	0.70	3.32	(0.59)	4.4	1.5	0.3–2.5	Stock 5F	C	1.60	2.83	(1.32)	0.9	0.4	0.0–1.2
NGC 7160B	C	0.70	3.08	(0.53)	4.5	1.6	0.4–2.7	Stock 5G	C	1.60	1.68	(0.56)	0.1	0.3	0.0–1.0
NGC 7160C	C	0.70	1.18	(0.22)	2.2	0.1	0.0–1.4	Stock 5H <sup>g,i</sup>	C	1.60	0.44	(0.05)	23.7	0.0	0.0–0.7
NGC 7160D	C	0.70	1.60	(0.53)	1.7	0.0	0.0–1.3	Stock 5I <sup>g,i</sup>	I	1.60	0.34	(0.04)	33.9	0.0	0.0–0.7
NGC 7160E	C	0.70	2.20	(0.91)	1.7	0.8	0.0–2.0	NGC 744A	C	1.50	3.06	(1.98)	0.8	1.5	0.7–2.4
NGC 7160F	I	0.70	1.01	(0.27)	1.2	0.1	0.0–1.4	NGC 744B	C	1.50	2.18	(0.30)	2.3	0.9	0.1–1.7
NGC 7160G	C	0.70	4.66	(1.31)	3.0	0.9	0.0–2.0	NGC 744C	C	1.50	3.27	(0.66)	2.7	0.9	0.1–1.7
NGC 7160H	C	0.70	1.67	(0.33)	2.9	0.4	0.0–1.6	NGC 744D	C	1.50	2.73	(0.74)	1.7	0.3	0.0–1.1
NGC 7160I	C	0.70	1.50	(1.03)	0.8	1.0	0.0–2.2	IC 1848G	I	2.31	3.57	(1.72)	0.7	3.3	2.3–4.5
NGC 7160J	I	0.70	1.20	(0.36)	1.4	0.5	0.0–1.7	NGC 1444B	C	1.00	1.16	(0.29)	0.6	2.8	1.6–4.3
NGC 7160K	C	0.70	9.89	(9.29)	1.0	1.3	0.0–2.4	NGC 1444K <sup>g</sup>	I	1.00	1.23	(0.23)	1.0	0.0	0.0–0.9
NGC 7160L	C	0.70	3.35	(1.39)	1.9	0.6	0.0–1.7	NGC 1444L <sup>g,h</sup>	C	1.00	3.43	(0.98)	2.5	0.0	0.0–0.4
NGC 7160M <sup>i</sup>	C	0.70	4.50	(1.11)	3.4	2.9	1.9–3.9	Bk 11A	I	2.20	2.94	(0.49)	1.5	5.1	3.0–8.2
NGC 7160N	C	0.70	4.93	(1.71)	2.5	2.8	1.9–3.8	Bk 11B <sup>h</sup>	C	2.20	1.96	(0.24)	1.0	5.5	3.2–8.8
NGC 7160O	C	0.70	6.48	(3.78)	1.5	2.5	1.4–3.4	Bk 11C	C	2.20	1.62	(0.59)	1.0	3.2	1.6–5.4
NGC 7160P	C	0.70	5.10	(2.06)	2.1	2.6	1.5–3.6	Bk 11F	I	2.20	2.18	(0.98)	0.0	0.1	0.0–1.4
NGC 7160Q	C	0.70	5.09	(1.64)	2.7	2.5	1.4–3.5	Bk 11G	I	2.20	1.37	(0.83)	1.0	1.1	0.0–2.7
NGC 7160R	C	0.70	4.30	(2.20)	1.6	2.8	1.8–3.8	NGC 1605A <sup>h</sup>	I	2.72	1.52	(0.22)	5.4	4.4	2.4–7.4
NGC 7380A	I	3.60	3.30	(0.62)	0.5	5.9	4.9–6.9	NGC 1893B	C	4.00	3.81	(2.39)	0.1	2.6	0.0–14.6
NGC 7380B <sup>h</sup>	I	3.60	3.06	(0.48)	1.1	5.6	4.6–6.7	NGC 1893C	C	4.00	2.00	(0.67)	3.0	1.4	0.0–9.7
NGC 7380C	C	3.60	3.77	(1.17)	0.1	5.8	4.8–6.9	NGC 1893D	I	4.00	1.09	(0.37)	7.9	3.6	0.0–16.0
NGC 7380D	I	3.60	3.27	(0.43)	0.8	5.3	4.3–6.3	NGC 1893E	C	4.00	4.92	(1.49)	0.6	3.9	0.0–25.0
Bk 59B	I	1.00	2.96	(0.69)	2.9	1.6	0.8–2.5	NGC 1931A	I	1.80	3.56	(0.77)	2.3	48.5	5.6–...
NGC 103A	I	3.03	1.67	(0.43)	3.2	3.2	2.3–4.2	NGC 2129A	I	2.00	2.36	(0.34)	1.1	0.4	0.0–6.3
NGC 281B	C	2.20	1.13	(0.25)	4.3	4.1	3.1–5.2	NGC 2129B	C	2.00	2.90	(0.64)	1.4	1.8	0.0–11.2
Bk 62A	I	2.05	3.28	(0.97)	1.3	4.2	3.2–5.3	NGC 2129C	I	2.00	1.21	(0.14)	5.8	3.3	0.0–21.8
Bk 62C	C	2.05	2.21	(0.47)	0.3	1.1	0.3–1.9	NGC 2175C	C	1.95	2.95	(0.57)	1.8	2.0	0.0–7.3
NGC 433A	I	4.50	2.90	(0.72)	2.2	2.0	1.1–2.9	NGC 2175D <sup>g</sup>	I	1.95	2.00	(0.54)	0.1	0.0	0.0–2.4
NGC 433B <sup>i</sup>	I	4.50	1.23	(0.29)	11.4	1.9	1.0–2.8	NGC 2175E	I	1.95	1.04	(0.17)	5.3	0.1	0.0–3.1
NGC 433C <sup>i</sup>	C	4.50	1.29	(0.29)	11.0	0.9	0.1–1.7								

<sup>a</sup> Adopted distance (see Table 4); equal to the distance of the cluster near which the cloud was discovered.

<sup>b</sup> Distance derived from the empirical line width–size relation, the observed CO line width, and the cloud angular size, the latter being particularly uncertain in cases of incompletely mapped clouds (*I*). The line width–size relation parameters obtained for class *A*, class *U*, and Dame *et al.* 1986 clouds (see Table 6) were used.

<sup>c</sup> One sigma error in  $d_{ls}$  derived from uncertainties in line width–size relation parameters, observed line width, and angular size.

<sup>d</sup> Number of sigma by which  $d_{ls}$  and  $d_{cl}$  differ (i.e.,  $\Delta \equiv |d_{ls} - d_{cl}|/\sigma_{d_{ls}}$ ).

<sup>e</sup> Kinematic distance based on the rotation curve of Brand 1986 and the observed Galactic longitude and radial velocity of the cloud.

<sup>f</sup> Kinematic distance range if a 10 km s<sup>-1</sup> component of the cloud velocity is due to Galactic noncircular motion.

<sup>g</sup> The Brand 1986 rotation curve does not predict a velocity equal to the observed cloud velocity. The quoted value of  $d_{kin}$  is the distance at which the velocity from the rotation curve is most nearly equal to that observed.

<sup>h</sup>  $d_{ls}$  significantly disagrees with  $d_{kin}$ .

<sup>i</sup> Both  $d_{ls}$  and  $d_{kin}$ , which are in reasonable agreement, are significantly discordant with  $d_{cl}$  ( $\Delta \geq 3$  and  $d_{cl}$  not in kinematic distance range), perhaps indicating that the cloud is not associated with the cluster which is its namesake.

distance from method (2) differs from the cluster distance. Eight of the clouds are at estimated distances that are so discrepant with those of the clusters (see criteria described in note “i” to Table 8) that their association with the clusters is considered unlikely. Locations of the remaining 69 class *a* clouds relative to the clusters remain ambiguous. Note that three of the four clouds that previously had been considered “possibly associated” with NGC 433, an “OB” cluster of uncertain age (see Paper I), are unlikely to be associated with the cluster.

Least-squares fits to the CO line width–mass–radius data were obtained for samples of clouds that include the class *a* clouds (see Tables 6 and 7). When appropriate stellar distances are assigned to the clouds, and the eight class *a* clouds considered not likely to be associated with clusters are disre-

garded, the derived fit parameters agree well with those obtained when the class *a* clouds are omitted, and the rms residuals with respect to the fit lines are reduced. On the contrary, the fit parameter values change, and the residual becomes larger, if kinematic distances and the same distance errors (50%) are assigned to the class *a* clouds.

#### b) Dependence of Cloud Properties on Cluster Age

In this section we report on differences in properties of clouds associated with clusters of different ages. Only class *A* and class *a* clouds are considered here. The eight class *a* clouds whose distances were found in the previous section to differ significantly from the cluster distances are excluded.

Frequency distributions of the sizes of molecular clouds

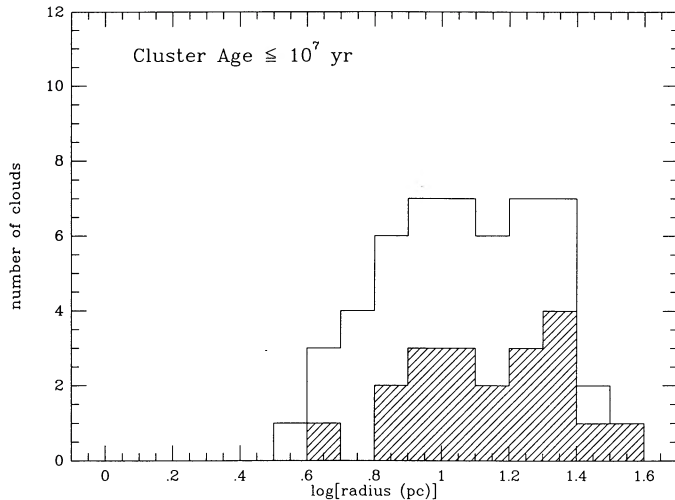


FIG. 16a

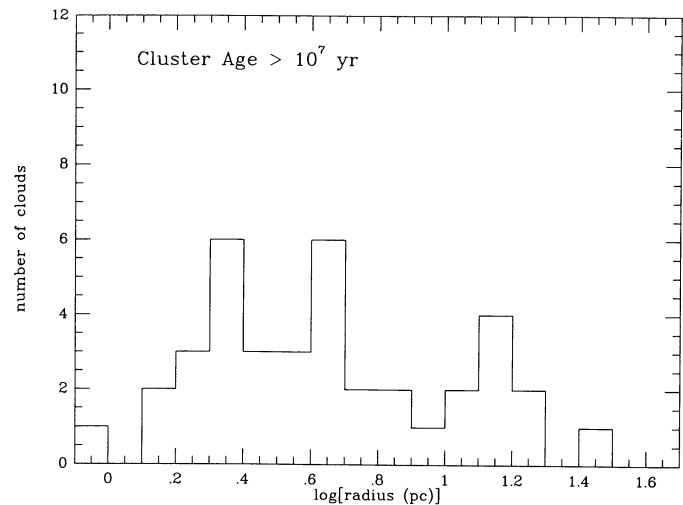


FIG. 16b

FIG. 16.—Size distributions for molecular clouds associated with open clusters of age (a) 10 Myr or younger, and (b) older than 10 Myr. The hatched histogram represents only class A clouds, those that are known with confidence to be associated with the clusters. Class a clouds, except the eight believed not to be associated with the clusters, are included in the unshaded histograms.

associated with clusters of different ages are shown in Figure 16. Figure 17 shows analogous distributions of cloud mass. The clouds associated with older clusters are smaller and less massive than the clouds associated with very young clusters. This general result was noted in the summary of Paper I.

If the gas in clouds associated with very young clusters is warmer than that in clouds found near older clusters because younger clusters contain more luminous stars, one might expect there to be a bias in inferred cloud mass via the dependence of the CO line intensity on gas kinetic temperature. To estimate the magnitude of this bias, we calculated the mean peak  $T_R^*$  in different cloud samples and found  $\langle T_R^*(\max) \rangle = 3.93 \pm 0.45$  (s.d.o.m.) K in clouds associated with clusters younger than 5 Myr,  $2.24 \pm 0.18$  (s.d.o.m.) K in those found near 5–20 Myr old clusters, and  $2.15 \pm 0.21$  (s.d.o.m.) K in those found near older clusters. The CO line radiation temperature increases in proportion not only to the gas kinetic temperature, but also to the beam filling fraction of emitting

clumps of gas in the cloud. Since the source-beam coupling could be greater in larger clouds due to the longer path length through the cloud in a typical line of sight, the measured contrast in  $\langle T_R^*(\max) \rangle$  among the various cloud samples sets an approximate upper limit on the variation in gas kinetic temperature. The much greater variation in cloud mass among samples of clouds associated with clusters of different ages apparently cannot be attributed in large measure to a variation in the gas kinetic temperature.

The observation that younger clusters have associated with them larger and more massive clouds than older clusters is consistent with a model in which OB clusters form in massive molecular clouds which are destroyed or dispersed within about 5–10 Myr of the time the O stars form (Paper I). In this picture, older clusters are presumed to have been at one time essentially the same as the clusters that presently contain O stars; they differ only in the sense that the massive stars have evolved away from the main sequence. If one were willing to

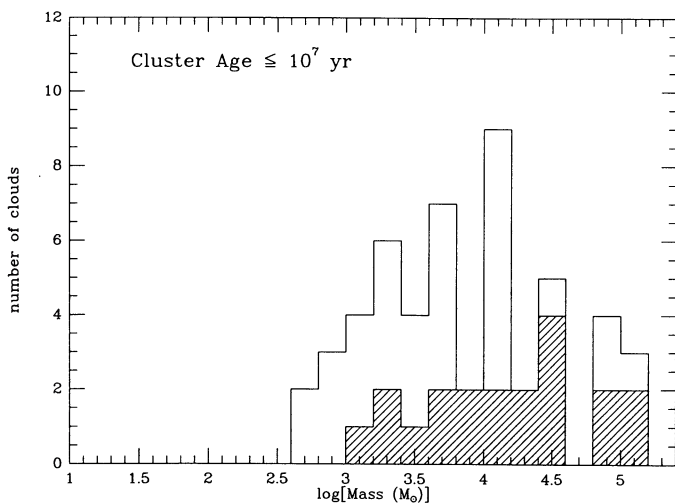


FIG. 17a

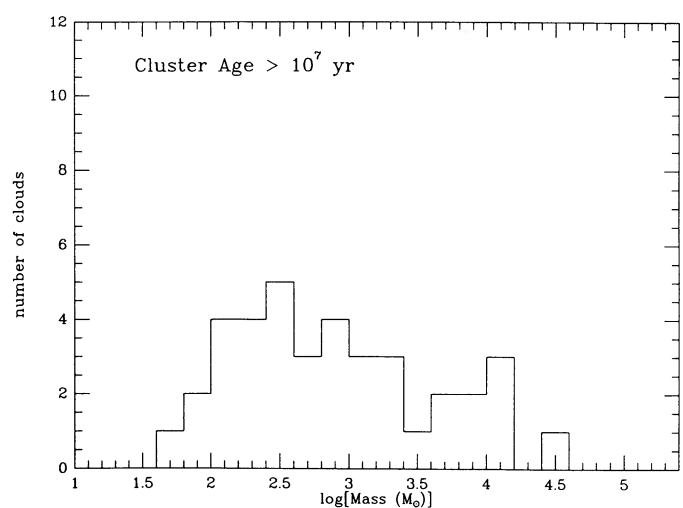


FIG. 17b

FIG. 17.—Same as Fig. 16, but showing distributions of cloud mass

part with this conventional notion, a second interpretation is possible in which the so-called older clusters actually differ from the “young” ones in that the ones that appear older never produced O stars. In this case, one would conclude that the mass of the most massive star that forms in a cluster increases with the mass of the cloud in which the cluster forms, a result that could be understood theoretically (Larson 1978; Elmegreen 1985).

*c) Do Clouds Associated with Clusters Differ from Local Dark Clouds?*

The same comparisons that were made of clouds associated with clusters of different ages can be made to address the question of whether clouds associated with clusters differ from the local dark clouds. Characteristics of the average local dark cloud found in the open cluster survey were given in Table 5. Frequency distributions of the sizes and masses of these clouds are shown in Figure 18. From Table 5 or a comparison of Figure 18 with Figures 16 and 17, it is clear that class *L* clouds are much smaller and less massive than the clouds associated with very young clusters, but they are similar in size and mass to the (class *a*) clouds that may be associated with older clusters.

The mean peak radiation temperature for the class *L* clouds is  $\langle T_R^*(\max) \rangle = 3.20 \pm 0.17$  (s.d.o.m.) K, roughly the same as that of the clouds associated with clusters (see above). The fact that the local clouds have slightly higher peak  $T_R^*$  than the class *a* clouds associated with clusters older than 5 Myr can be explained by the greater beam dilution suffered by clouds in the latter group due to their greater distances. The class *A* clouds associated with clusters younger than 5 Myr also are more distant than the local clouds, so the fact that class *A* clouds are characterized by a higher peak  $T_R^*$  despite the effect of beam dilution may be taken as evidence that these clouds indeed are warmer.

Although in our catalog there are too few completely mapped local dark clouds with distance estimates to measure accurately the size or mass spectrum, the number of local clouds falls off with increasing size at a rate indistinguishable

from that pertaining to clouds associated with clusters. The distributions differ only in ways that can be understood as due to differences in completeness (see § IIIc).

The line width–size and mass–size relations give an ambiguous answer to the question raised in this section. As can be seen in Figure 12a, the local dark clouds tend to be too small for their line widths, or to have line widths that are too large for their sizes, relative to the line width–size relation that best describes the cataloged clouds (eq. [8]). This apparent discrepancy would vanish if many of the local clouds were more distant than they are believed to be. While the distances of these clouds are poorly known, we do not suspect that they have been underestimated systematically.

Another possible explanation for the anomalous appearance of local dark clouds suggested by their relatively small sizes (see Table 5) is that CO self-absorption has begun to occur due to the smaller clump–clump velocity dispersion predicted by the line width–size relation. Some degree of self-absorption might also account for the finding of Carr (1987) and Loren (1989a) that clumps in the Cepheus and Ophiuchus clouds are described by relatively shallow line width–size relation slopes. The problem with this explanation is that self-absorption should result in underestimation of the cloud mass, yet the inferred masses of local dark clouds are too large for their sizes compared to the derived mass–radius relation (see Fig. 13).

The possibility remains that flattening of the line width–size relation for clouds smaller than a few parsecs in radius occurs because small clouds differ physically from larger ones. The derived masses and observed CO line widths of the local dark clouds suggest that these clouds might be a factor of about 4 denser than the 20 or so  $H_2$  molecules per  $cm^3$  mean density estimated for larger clouds. If the small, dense clouds resemble the clumps of which the larger clouds are made, the class *L* clouds could be by-products of the destruction of larger clouds or the ingredients from which a future generation of large clouds will form.

In summary, we find no compelling reason to suppose that local dark clouds differ in any significant way from the molecular clouds associated with open clusters, though a complete explanation of why the local clouds *appear* not to agree with

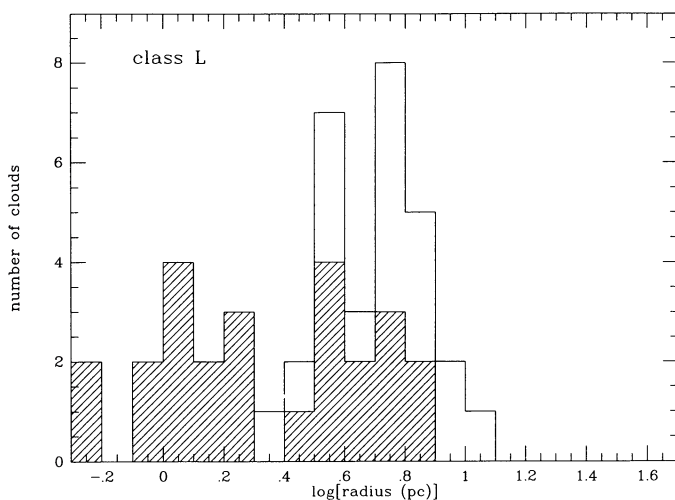


FIG. 18a

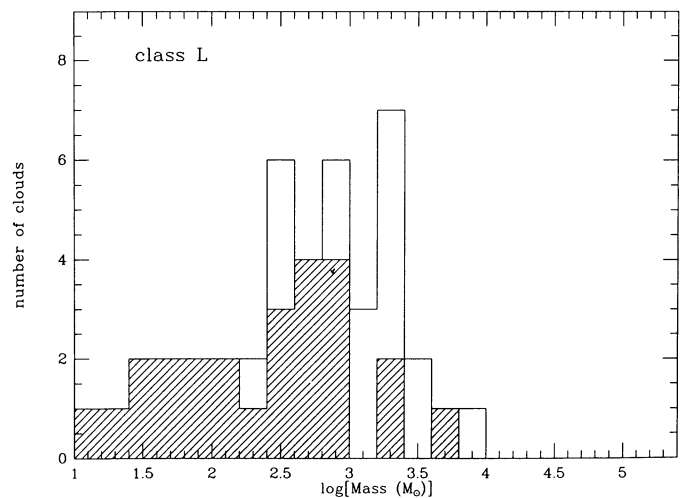


FIG. 18b

FIG. 18.—(a) Size and (b) mass distributions of local dark clouds. Those clouds with measured distances are represented with the hatched histograms. Included in the upper histograms are the 17 clouds with distance upper limits. The sizes and masses of clouds in the latter category are upper limits.

the line width–radius and mass–radius relations delineated by the clouds associated with clusters remains elusive.

## VI. CONCLUSIONS

We have examined the physical properties of the 148 molecular clouds found in our CO survey of regions around 34 young open clusters with the following principal results:

1. The molecular cloud size spectrum can be described approximately by  $N(R > R_0) \propto R_0^{-1.6}$  for  $8 \text{ pc} < R_0 < 20 \text{ pc}$ . This result was derived from the frequency distribution of radii of completely mapped clouds in a range of cloud sizes to which the survey is thought to be equally sensitive. An analogous derivation of the cloud mass spectrum indicates  $N(M > M_0) \propto M_0^{-0.65}$  for  $2.0 \times 10^3 M_\odot < M_0 < 1.3 \times 10^5 M_\odot$ .

2. The clouds are distinctly nonspherical and appear to be randomly oriented with respect to the Galactic plane. The hypothesis that a cloud has equal probability of alignment with any Galactic position angle cannot be rejected.

3. All the observations discussed in this paper can be explained by a model for molecular clouds in which clouds are supposed to be ensembles of dense clumps of gas. The mean  $\text{H}_2$  volume densities of molecular clouds are much lower than the critical density required for collisional excitation of CO molecules, and the maximum antenna temperature measured in each cloud is lower than any plausible estimate of the gas kinetic temperature. Hence, either the  $^{12}\text{CO } J = 1 \rightarrow 0$  line is not optically thick and “thermalized,” as it is widely believed to be, or the line-emitting gas is in small, dense clumps that fill only about 1% of the cloud volume. The latter interpretation is favored because it is known from irregularities in millimeter spectral line intensity maps that molecular clouds are inhomogeneous on all scales yet resolved. In this picture, the CO line width measures the one-dimensional clump-clump velocity dispersion because the velocity dispersion generally far exceeds the clump thermal line width; when this condition is satisfied, the CO line is not saturated, and it can be used effectively as a probe of  $\text{H}_2$  column density. If the factor by which  $T_R^*$  ( $= T_A^*/\eta_{\text{FSS}}$ ) underestimates the gas kinetic temperature is a measure of the fraction of the telescope beam filled by clumps (at a given radial velocity), the low peak antenna temperatures measured in the best resolved clouds in our catalog imply clump radii of the order of 0.3 pc or less.

4. Power laws with slopes of 0.6 and 3 are found to describe, respectively, the relations of CO line width and cloud mass to cloud size. The mass–radius relation differs markedly from the form reported elsewhere in the literature, and we ascribe much of the discrepancy to the systematic bias introduced when the effect of correlated errors is neglected. Errors in mass and radius are correlated because both depend upon distance. The correlation of errors must be taken into account because the distances of molecular clouds are not known with great accuracy. A corollary to the derived relation  $M \propto R^3$  is that the mean cloud volume density is roughly constant: clouds of all sizes in our catalog have a mean density of about  $20 \text{ H}_2$  molecules per  $\text{cm}^3$ .

5. Molecular clouds are not in virial equilibrium insofar as they do not have CO line widths equal to the “virial velocity,”  $(3GM/5R)^{1/2}$ , where  $M$  and  $R$  denote, respectively, cloud mass

and radius. This is implicit in the mass–radius and line width–radius relation slopes and is further demonstrated in a comparison of the observed CO line widths with the virial velocities of individual clouds. Small clouds are found to be farther from virial equilibrium than larger ones, but even the largest cataloged clouds have line widths approximately equal to the escape velocity  $(2GM/R)^{1/2}$ .

6. An assessment of the time scales on which clumpy molecular clouds are perturbed and relax, and of the cloud lifetimes, may be consistent with the observation that clouds appear to be out of equilibrium. The relaxation of a perturbed cloud to virial equilibrium occurs slowly relative to the perturbation time or the cloud lifetime provided that, in a single collision of two clumps, the relative trajectory is not drastically bent. We introduce a collision strength parameter,  $\Omega$ , which can be used to decide if relaxation to virial equilibrium is likely. Since clouds are not in virial equilibrium, we predict that  $\Omega$  is greater than or about equal to 30. In principle, this prediction can be tested with sophisticated numerical simulations of clump-clump collisions.

7. The local dark clouds found in the open cluster survey appear to differ from the clouds associated with clusters. Some, but not all, of the differences can be explained by observational selection effects. For instance, the average local cloud is smaller and less massive than the average cloud associated with a cluster, but a physically large local cloud might subtend too great a solid angle to fit in a surveyed region. On the other hand, the masses and CO line widths of the local clouds are larger than expected for their sizes based on the observations of clouds associated with clusters. These apparent discrepancies can be explained if the distances of the local clouds were systematically underestimated by a large factor, which is doubtful, or if the local clouds are relatively dense and CO line saturation has led to overestimation of the line widths. In the latter case, the relatively small local clouds may resemble the clumps in larger clouds.

8. For reasons that cannot be attributed to observational selection effects, we find that the molecular clouds associated with open clusters younger than 10 Myr are significantly larger and more massive than the ones associated with older clusters. This conclusion would be strengthened if some of the clouds classified as type *a*, whose association with a cluster cannot be firmly established, are actually not associated.

Stimulating conversations with Dave Bazell, Tom Dame, Bob Dickman, Eli Dwek, Neal Evans, John Scalo, and Tom Sodroski led to improvements in the discussion sections of this paper. Frank Bash, Mike Hauser, and Tom Kelsall reviewed a draft of the paper and provided many helpful comments. The author thanks these colleagues and the referee, Marc Kutner, for sharing their insights. Thanks also to Pat Thaddeus for his generous allocation of telescope time to the open cluster survey. Most of all, thanks to Frank Bash who suggested the project initially, and then provided guidance and support as it was carried out. Partial funding support was provided by the National Science Foundation under grant AST 8815801 and by the National Aeronautics and Space Administration under ADP grants R033-87 and R033-88.

## REFERENCES

- Allen, C. W. 1973, *Astrophysical Quantities* (London: Athlone).
- Alter, G., Ruprecht, J., and Vanysek, V. 1970, *The Catalog of Star Clusters and Associations* (Budapest: Akademia Kiado).
- Barnard, E. D. 1927, *Carnegie Institution of Washington Publication*, No. 247, Part I.
- Bash, F. N., Hausman, M. A., and Papaloizou, J. 1981, *Ap. J.*, **245**, 92.
- Bash, F. N., and Peters, W. L. 1976, *Ap. J.*, **205**, 786.
- Blitz, L., and Shu, F. H. 1980, *Ap. J.*, **238**, 148.
- Bloemen, J. B. G. M., Caraveo, P. A., Hermsen, W., Lebrun, F., Maddalena, R. J., Strong, A. W., and Thaddeus, P. 1984, *Astr. Ap.*, **139**, 37.
- Bonazzola, S., Falgarone, E., Heyvaerts, J., Pérault, M., and Puget, J. L. 1987, *Astr. Ap.*, **172**, 293.
- Brand, J. 1986, Ph.D. thesis, Rijksuniversiteit te Leiden.
- Carr, J. S. 1987, *Ap. J.*, **323**, 170.
- Casoli, F., Combes, F., and Gerin, M. 1984, *Astr. Ap.*, **133**, 99.
- Chandrasekhar, S. 1942, *Principles of Stellar Dynamics* (Chicago: University of Chicago Press).
- Chièze, J. P. 1987, *Astr. Ap.*, **171**, 225.
- Clemens, D. P., and Barvainis, R. 1988, *Ap. J. Suppl.*, **68**, 257.
- Clifford, P., and Elmegreen, B. G. 1983, *M.N.R.A.S.*, **202**, 629.
- Dame, T. M. 1983, Ph.D. thesis, Columbia University.
- Dame, T. M., Elmegreen, B. G., Cohen, R. S., and Thaddeus, P. 1986, *Ap. J.*, **305**, 892.
- Dame, T. M., and Thaddeus, P. 1985, *Ap. J.*, **297**, 751.
- Dame, T. M., et al. 1987, *Ap. J.*, **322**, 706.
- David, M., and Leisawitz, D. 1990, in preparation.
- David, M., and Verschueren, W. 1987, *Astr. Ap.*, **186**, 295.
- Dickman, R. L., Snell, R. L., and Schloerb, F. P. 1986, *Ap. J.*, **309**, 326.
- Elmegreen, B. G. 1985, in *Protostars and Planets II*, ed. D. C. Black and M. S. Matthews (Tucson: University of Arizona Press), p. 33.
- . 1989, *Ap. J.*, **338**, 178.
- Evans, N. J. II. 1980, in *IAU Symposium 87, Interstellar Molecules*, ed. B. H. Andrew (Dordrecht: Reidel), p. 1.
- Falgarone, E., and Pérault, M. 1988, *Astr. Ap.*, **205**, L1.
- Falgarone, E., and Puget, J. L. 1985, *Astr. Ap.*, **142**, 157.
- . 1986, *Astr. Ap.*, **162**, 235.
- Ferrière, K. M., Zweibel, E. G., and Shull, J. M. 1988, *Ap. J.*, **332**, 984.
- Fleck, R. C., Jr. 1983, *Ap. J. (Letters)*, **272**, L45.
- . 1988, *Ap. J.*, **328**, 299.
- Frerking, M. A., Langer, W. D., and Wilson, R. W. 1987, *Ap. J.*, **313**, 320.
- Gilden, D. L. 1984, *Ap. J.*, **279**, 335.
- Goldsmith, P. F. 1987, in *Interstellar Processes*, ed. D. J. Hollenbach and H. A. Thronson, Jr. (Dordrecht: Reidel), p. 51.
- Hausman, M. A. 1981, *Ap. J.*, **245**, 72.
- Heiles, C. 1987, in *Interstellar Processes*, ed. D. J. Hollenbach and H. A. Thronson, Jr. (Dordrecht: Reidel), p. 171.
- Jefferys, W. H. 1980, *A.J.*, **85**, 177.
- Kegel, W. H. 1989, preprint.
- Kleiner, S. C., and Dickman, R. L. 1985, *Ap. J.*, **295**, 466.
- Kutner, M. L. 1978, *Ap. Letters*, **19**, 81.
- . 1984, *Fund. Cosmic Phys.*, **9**, 233.
- Kutner, M. L., and Ulich, B. L. 1981, *Ap. J.*, **250**, 341.
- Larson, R. B. 1978, *M.N.R.A.S.*, **184**, 69.
- . 1981, *M.N.R.A.S.*, **194**, 809.
- Lee, Y., Snell, R. L., and Dickman, R. L. 1990, *Ap. J.*, **355**, 536.
- Leisawitz, D. 1985, Ph.D. thesis, University of Texas at Austin.
- . 1988, *Catalog of Open Clusters and Associated Interstellar Matter*, NASA Reference Publication RP-1202.
- Leisawitz, D., Bash, F. N., and Thaddeus, P. 1988, *Ap. J. Suppl.*, **70**, 731 (Paper I).
- Leisawitz, D., and Klinglesmith, D. A. 1989, in *Molecular Clouds in the Milky Way and External Galaxies*, ed. R. Dickman, R. Snell, and J. Young (Berlin: Springer-Verlag), p. 99.
- Leung, C. M., Kutner, M. L., and Mead, K. N. 1982, *Ap. J.*, **262**, 583.
- Loren, R. B. 1989a, *Ap. J.*, **338**, 902.
- . 1989b, *Ap. J.*, **338**, 925.
- Lynds, B. T. 1962, *Ap. J. Suppl.*, **7**, 1.
- Maloney, P. 1988, *Ap. J.*, **334**, 761.
- . 1990, *Ap. J. (Letters)*, **348**, L9.
- Mead, K. N., and Kutner, M. L. 1988, *Ap. J.*, **330**, 399.
- Myers, P. C. 1983, *Ap. J.*, **270**, 105.
- . 1987, in *Interstellar Processes*, ed. D. J. Hollenbach and H. A. Thronson, Jr. (Dordrecht: Reidel), p. 71.
- Myers, P. C., and Benson, P. J. 1983, *Ap. J.*, **266**, 309.
- Myers, P. C., and Goodman, A. A. 1988, *Ap. J. (Letters)*, **326**, L27.
- Norman, C., and Silk, J. 1980, *Ap. J.*, **238**, 158.
- Pumphrey, W. A., and Scalo, J. M. 1983, *Ap. J.*, **269**, 531 (PS).
- Sanders, D. B., Scoville, N. Z., and Solomon, P. M. 1985, *Ap. J.*, **289**, 373.
- Savage, B. D., and Mathis, J. S. 1979, *Ann. Rev. Astr. Ap.*, **17**, 73.
- Scalo, J. M. 1985, in *Protostars and Planets II*, ed. D. C. Black and M. S. Matthews (Tucson: University of Arizona Press), p. 201.
- . 1987, in *Interstellar Processes*, ed. D. J. Hollenbach and H. A. Thronson, Jr. (Dordrecht: Reidel), p. 349.
- Scalo, J. M., and Pumphrey, W. A. 1982, *Ap. J. (Letters)*, **258**, L29.
- Silk, J. 1988, in *Galactic and Extragalactic Star Formation*, ed. R. E. Pudritz and M. Fich (Dordrecht: Kluwer), p. 503.
- Solomon, P. M., Rivolo, A. R., Barrett, J., and Yahil, A. 1987, *Ap. J.*, **319**, 730.
- Spitzer, L., Jr., and Härm, R. 1958, *Ap. J.*, **127**, 544.
- Stark, A. A. 1979, Ph.D. thesis, Princeton University.
- Stone, M. E. 1970, *Ap. J.*, **159**, 293.
- Strong, A. W., et al. 1988, *Astr. Ap.*, **207**, 1.
- Terebey, S., Fich, M., Blitz, L., and Henkel, C. 1986, *Ap. J.*, **308**, 357.
- Vogel, S. N., Kulkarni, S. R., and Scoville, N. Z. 1988, *Nature*, **334**, 402.
- Woolfson, M. M. 1978, in *The Origin of the Solar System*, ed. S. F. Dermott (New York: John Wiley), p. 163.
- Wu, Y., and Evans, N. J. II. 1989, *Ap. J.*, **340**, 307.
- Zuckerman, B., and Evans, N. J. II. 1974, *Ap. J. (Letters)*, **192**, L149.

DAVID LEISAWITZ: Infrared Astrophysics Branch, Code 685, NASA Goddard Space Flight Center, Greenbelt, MD 20771